
FEMLAB Model of a Coupled Electromagnetic-Thermal Boundary Value Problem

Submitted & Approved: July 29, 2005

Revised: July 10, 2006

Christopher Mirabito

Department of Mathematical Sciences
Wean Hall, Room 6113
Carnegie Mellon University
Pittsburgh, PA 15213-3890
cmirabit@andrew.cmu.edu

Anu Narayanan

Department of Mathematics
University of Texas at Austin
1 University Station C1200
Austin, TX 78712-0257
n.anupama@gmail.com

David Pérez

Department of Mathematics
Suite 2700, University Hall
Loyola Marymount University
1 LMU Drive
Los Angeles, CA 90045
dperez7@lion.lmu.edu

Brenton Stone

Department of Mathematics
University at Buffalo
The State University of New York
244 Mathematics Building
Buffalo, NY 14260-2900
brstone2@buffalo.edu

Professor Suzanne L. Weekes, Advisor

Professor Vadim Yakovlev, Advisor



This research was sponsored by the National Science Foundation (NSF), jointly with the Worcester Polytechnic Institute (WPI), the Center for Industrial Mathematics and Statistics (CIMS), and The Ferrite Company, Inc. The views and conclusions contained in this document are those of the authors and should not be interpreted as representing the official policies, either expressed or implied, of WPI, CIMS, Ferrite, the NSF, or the U.S. Government.

Abstract

In a microwave oven, food is heated as a result of two simultaneous physical processes: absorption of electromagnetic energy and heat diffusion. It is known from experience that microwave heating can often be very nonuniform and difficult to control. A system of coupled partial differential equations modeling these two phenomena is formulated, but it is impossible to solve exactly except in trivial cases.

We investigate the use of the finite element method software FEMLAB in obtaining numerical solutions to our coupled system.

Acknowledgments

We would like to thank our advisors, Professors Suzanne Weekes and Vadim Yakovlev, for providing valuable guidance throughout the course of this project. They showed genuine interest in our progress; our meetings every morning stand testament to this. Their hopes for the project and their faith in our abilities made all the hard work meaningful.

We would like to thank The Ferrite Company, Inc. for giving us an interesting problem for the summer. We especially want to thank Mr. Eugene Eves, Vice President of Research and Development at Ferrite, for meeting with us and providing direction whenever necessary.

We wish to thank Professor Darko Volkov for helping us with some problems we encountered early in the process and Professor Alex Zozulya from the WPI Department of Physics for taking time to explain some theoretical ideas. We would also like to thank Professor Arthur Heinricher, who inspired us to explore new aspects of our problem by posing thought-provoking questions.

We greatly appreciate the contributions of the REU Research Assistant, Rebecca Wasyk. From exposing us to the finite element method to driving us to the grocery store, Becky truly offered her services in all aspects of the program. We also thank the other REU students for being our audience during weekly presentations.

Finally, we would like to thank the Center for Industrial Mathematics and Statistics (CIMS) at WPI for supporting this REU and the National Science Foundation (NSF) for funding the program.

Contents

1	Introduction	1
1.1	A Brief History of Microwave Heating	1
1.2	ISM Frequencies	2
1.3	An Overview of Microwave Oven Components	2
2	Electromagnetic Waves	4
2.1	Maxwell's Equations	4
2.1.1	Derivation of the Wave Equation	5
2.1.2	Time-Harmonic Fields and the Helmholtz Equations	6
2.2	EM Boundary Conditions	7
2.2.1	Dielectric-Dielectric Boundary Conditions	8
2.2.2	Conductor-Dielectric Boundary Conditions	8
2.2.3	Input Port Boundary Condition	9
2.3	Energy Considerations	9
2.4	Exact Solution for an Empty Waveguide	9
2.5	Power of a TE ₁₀ Mode	12
3	Heat Diffusion	14
3.1	Formulation of the Heat Equation	14
3.1.1	Fourier's Law of Conduction	14
3.1.2	Heat Flow Across a Surface	14
3.1.3	Rate of Change of Total Heat	15
3.1.4	Law of Conservation of Energy	15
3.1.5	Electromagnetic Heating	16
3.2	Boundary Conditions	16
3.2.1	Load-Waveguide and Load-Air Interfaces	16
3.2.2	Load-Load Interface	16
3.3	Governing Equations	16
4	Implementation in FEMLAB	18
4.1	Common Elements of Our Models	18
4.2	Layout of the Model in FEMLAB	18
4.3	Implementation of Governing Equations in FEMLAB	19
4.3.1	Electromagnetic Waves	19
4.3.2	Heat Transfer	21
4.4	Material Constants	21
4.5	Solving the Model	24
4.5.1	The Nyquist Criterion	24
4.5.2	Choice of Linear System Solver	24

5 Numerical Experiments and Results	26
5.1 Accuracy of FEMLAB's EM Field Solution	26
5.2 Role of Thermal Diffusion	26
5.3 Temperature Dependence of ϵ' and ϵ''	29
5.4 A Pulsing Power Source	30
5.4.1 Motivation	30
5.4.2 Implementation in FEMLAB	31
5.4.3 Pulsing Results	32
6 Conclusions	34
6.1 Limitations of FEMLAB	34
7 Future Work	35
A Dielectric and Thermal Properties of Loads	36
A.1 Almond	36
A.2 Golden Delicious Apple	37
A.3 Red Delicious Apple	37
A.4 Baked Potato	38
A.5 Ceramic Materials	38
A.6 Cheese Sauce	39
A.7 Cherry	39
A.8 Codling Moth	40
A.9 Cooked Beef	40
A.10 Cooked Beef Juice	41
A.11 Cooked Carrots	41
A.12 Cooked Ham	42
A.13 Cooked Macaroni Noodles	43
A.14 Cooked Turkey	43
A.15 Cooked Turkey Juice	44
A.16 Corn Oil	44
A.17 Cottage Cheese	45
A.18 Flour	45
A.19 Grapefruit	46
A.20 Indian-Meal Moth	46
A.21 Liquid Whey Protein Mixture	47
A.22 Macaroni and Cheese	47
A.23 Mashed Potato	48
A.24 Mexican Fruit Fly	49
A.25 Naval Orange Worm	49
A.26 Orange	50
A.27 Raw Beef	50
A.28 Raw Turkey	51
A.29 Skimmed Milk Powder	52
A.30 Solid Potato	52
A.31 Tap Water	53
A.32 Walnut	54
A.33 Whey Protein Gel	54
B Notation Used	55

List of Figures

2.1	A generic surface S , with boundary ∂S	7
2.2	A typical material interface, shown in 3D.	8
3.1	The Law of Conservation of Energy, stated in verbal form.	15
3.2	A heterogeneous load inside a waveguide.	17
4.1	Subdomains and boundaries used for our model in FEMLAB.	19
4.2	The Constants dialog box in FEMLAB.	20
4.3	The Subdomain Settings dialog box in the Electromagnetics Module of FEMLAB.	20
4.4	The Boundary Expressions dialog box in the Electromagnetics Module in FEMLAB.	21
4.5	FEMLAB's Boundary Settings dialog box for EM waves, located in the Electromagnetics Module. . .	22
4.6	The Subdomain Settings dialog box, located in the Heat Transfer Module.	23
4.7	Solve time vs. d	25
4.8	Memory usage vs. d	25
5.1	<i>QuickWave-3D</i> 's solution for $\ \vec{E}\ $	27
5.2	FEMLAB's solution for $\ \vec{E}\ $	27
5.3	Heating profiles for baked potato.	27
5.4	Loss factor ϵ'' vs. time for tap water to reach 100°C.	30
5.5	Temperature distribution inside tap water at $t = 5$	31
5.6	A dynamically pulsing function for $P(t)$	32
5.7	Results of T_{\max} versus t with a tap water load.	33

List of Tables

1.1	Selected ISM frequencies and region(s) where in use.	2
3.1	The system of governing equations and boundary conditions for Figure 3.2.	17
4.1	Calculated cutoff frequencies for selected TE modes in a WR975 waveguide.	18
4.2	Pros and cons of small and large values of d .	25
4.3	Parameters used in experimenting with drop tolerance values.	25
5.1	Results for simulations without diffusion ($K = 0$) and with diffusion ($K > 0$).	28
5.2	Temperature range data for $K = 0$ and $K > 0$.	28
5.3	Model parameters used in the one-way coupling vs. two-way coupling experiment.	29
5.4	Elapsed time for tap water to boil for set values of ϵ' and ϵ'' with given constant values of T .	29

Chapter 1

Introduction

Our project is concerned with microwave thermal processing. Conventional microwave ovens have been household necessities for the last three decades. Most consumers use microwave ovens in their kitchens mainly for cooking and reheating various food products, such as water for coffee or tea, meats, and popcorn. Many people prefer to use microwave ovens over traditional ranges because of the speed at which the food is heated.

Microwave heating is used not only in the home, but also in industry. Our industrial sponsor for this project, The Ferrite Company, Inc. of Nashua, NH, produces industrial microwave heating systems and many different microwave oven components. Founded in 1982, Ferrite designs and produces microwave systems that are used for industrial cooking, batch tempering, and drying. The company is committed to researching and developing methods to design more efficient heating systems that can heat food more uniformly. The food processing industry serves as the main customer for these systems.

Microwave heating can be explained as a combination of electromagnetic (EM) and thermodynamic phenomena. There exist materials, called lossy dielectrics, such that when an EM wave passes through them, it loses energy to the material. This energy is turned to heat inside the material. At the same time, there is heat flow within the material that acts toward eliminating temperature differences. The distribution of heat, nevertheless, will typically be nonuniform.

Our goal is to use FEMLAB, a software package based on the finite element method for solving partial differential equations, to simulate microwave heating. We model both the EM wave propagation and heat transfer. We limit ourselves to heat transfer by conduction, and we neglect the effects of convection and radiation to simplify the model.

Much of what is discussed in the following two chapters of this report concerns the electromagnetic and heat conduction theory needed to study how microwave ovens heat food.

1.1 A Brief History of Microwave Heating

The earliest real-world use of microwaves was in communication and radar systems during World War II [10]. Early research on the properties of dielectrics in the presence of EM waves was done by E. E. W. Kassner in the late 1930s and by A. von Hippel in the 1940s [9]. It was not until after the war had ended that significant study of microwave heating was undertaken. Pioneering work on microwave heating was done by P. Spencer of Raytheon in 1947. However, the story of his discovery of microwave cooking by accidentally leaning against an open-ended waveguide and noticing that a candy bar in his pocket had melted is apocryphal [9].

Upon hearing of Spencer's group's discovery of the new application for microwave heating, management at Raytheon was eager to exploit it. They developed the first commercially available microwave oven, the RadarangeTM. Raytheon marketed these ovens to commercial kitchens in restaurants. They became the dominant company in the field of microwave ovens until the middle of the 1960s [9].

There was a short-lived period of high demand for microwave systems in industrial applications during the early 1960s, which fell off after 1968. Applications included potato chip drying, vacuum and nylon fiber drying, highway paint drying, alcohol evaporation, urethane foam heating, sand core cooking, and chicken cooking [9]. As interest for industrial use waned, most of the leading microwave companies of the era invested in the consumer oven market. Consumer oven sales skyrocketed from less than 10,000 units *per annum* in 1966 to more than 1,000,000 units *per annum* by 1975 [9]. By 1983, the business was well-established, and today more than 90% of households in the United States contain a microwave oven.

Band	Region(s)
433.92 \pm 0.87 MHz	1
915. \pm 13. MHz	2
2.45 \pm 0.05 GHz	1, 2, 3
5.8 \pm 0.075 GHz	1, 2, 3
24.125 \pm 0.125 GHz	1, 2, 3
61.25 \pm 0.25 GHz	1, 2, 3
122.5 \pm 0.5 GHz	1, 2, 3
245. \pm 1. GHz	1, 2, 3

Table 1.1. Selected ISM frequencies and region(s) where in use.

Meanwhile, the industrial microwave heating market stagnated. During the 1970s and early 1980s, the market only grew slowly. Among the reasons for this were economics and fear of the effects of microwave radiation¹ [9]. Indeed, few companies, including Raytheon, Cober, and Microdry, remained invested in the field. Nevertheless, many more industrial applications were tried.

Most of the industrial microwave heating systems manufactured today are produced by small niche companies for customer-specific uses. Ferrite is one of such firms. Microwave heating now enjoys widespread acceptance both among consumers and in industry.

1.2 ISM Frequencies

The Industrial, Scientific, and Medical (ISM) frequencies are a listing of all EM wave frequency allocations for applications which are not used for radio communication. They include frequencies in which microwave applications are allowed to operate in various regions across the world. Any device emitting electromagnetic radiation using one of these frequencies does not need a Federal Communications Commission (FCC) license to operate. The main purpose of these frequencies is to minimize the amount of interference that can occur between many items that rely on EM waves, such as GSM cellular telephones and wireless computer networking systems [9].

A few ISM frequencies are shown in Table 1.1. In the table, Region 1 consists of Europe, Africa, Turkey, the Arabian Peninsula, the Middle East (except Iran), Siberia, and Mongolia. Region 2 consists of North and South America. Region 3 covers most of Asia, Australia, and Oceania [9]. The two frequencies most commonly used in microwave heating applications are 915 MHz and 2.45 GHz. It is worth noting that Ferrite uses 915 MHz in the development of most of its industrial microwave oven systems. As such, for the remainder of our project and throughout this report, we adopt a frequency of 915 MHz; all material properties listed in this report are held for 915 MHz unless explicitly stated otherwise.

1.3 An Overview of Microwave Oven Components

A conventional microwave heating system consists of four major components: the magnetron, the waveguide, the cavity (or applicator), and the load.

The magnetron generates EM waves. An anode-cathode system induces an electric field, while two ring magnets produce a magnetic field perpendicular to the electric field. The magnetron creates a high frequency alternating current, which in turn produces an EM wave. In our project, we will be running simulations of microwave heating using both a constant power output from the magnetron, as well as a time-dependent (pulsing) power output.

The waveguide is a metal tube that transmits and guides the EM waves from the magnetron into the cavity, which is the actual place of heating in a microwave oven. Waveguides come in many different shapes and sizes. However, most waveguides have either a circular or a rectangular cross-section. In our model, we will only consider rectangular waveguides.

¹Around this time there was much speculation, driven by both the media and Consumers Union, a nonprofit consumer advocacy group and publisher of *Consumer Reports*, that microwave radiation was harmful to one's health, especially to those who had pacemakers. This caused widespread fear of microwave ovens among consumers and industry alike. These allegations were promptly dismissed by scientists and eventually by the general public as largely unsubstantiated. Consumers Union has since dropped its warnings on microwave ovens [9].

The substance being heated is often referred to as the load. In our model, we place the load inside the waveguide, not in a separate cavity. It is the dielectric and thermal properties of the load that play an important role in how it heats. We discuss these different properties in detail throughout the report.

Chapter 2

Electromagnetic Waves

The first step that we need to take in this project is formulating a mathematical model of the system of partial differential equations and boundary conditions. This process is discussed in detail in the next two chapters, and it involves an in-depth study of the two processes that govern microwave heating: electromagnetic wave propagation and heat diffusion. We begin by exploring electromagnetic waves and their behavior. In this chapter, we discuss Maxwell's equations, formulate the wave equation and one form of the Helmholtz equation and its solution. Later in the chapter, we discuss electromagnetic boundary conditions and energy considerations.

2.1 Maxwell's Equations

Maxwell's equations govern electromagnetic phenomena. In a medium, they are as follows:

$$\nabla \cdot \vec{D} = \rho, \quad (2.1)$$

$$\nabla \times \vec{E} = -\frac{\partial \vec{B}}{\partial t}, \quad (2.2)$$

$$\nabla \cdot \vec{B} = 0, \quad (2.3)$$

$$\nabla \times \vec{H} = \vec{J} + \frac{\partial \vec{D}}{\partial t}, \quad (2.4)$$

where

$$\vec{D} = \epsilon' \epsilon_0 \vec{E}, \quad (2.5)$$

$$\vec{B} = \mu' \mu_0 \vec{H}, \quad (2.6)$$

$$\vec{J} = \sigma \vec{E}. \quad (2.7)$$

In equations (2.1) through (2.7), \vec{E} is the intensity of the electric field, \vec{B} is the magnetic flux density, ρ is the electric charge density, \vec{J} is the electric current, σ is the electrical conductivity, \vec{D} is the electric displacement (or the electric flux density), \vec{H} is the intensity of the magnetic field, $\epsilon_0 = 8.854 \times 10^{-12} \text{ F/m}$ is the permittivity of free space, ϵ' is the relative permittivity (also called the dielectric constant), $\mu_0 = 4\pi \times 10^{-7} \text{ N/A}^2$ is the permeability of free space, and μ' is the relative permeability.

Equation (2.1) is commonly called Gauss's Law. Equation (2.2) is known as Faraday's Law of Induction, which states that an electric field is induced by a time-dependent magnetic field. Equation (2.3) is called Gauss's Law of Magnetism, and disproves the existence of magnetic monopoles; there is no change in magnetic flux in a closed volume. Equation (2.4) is known as Ampère's Law, and this law says that magnetic fields are induced by electric currents as well as time-dependent electric fields. Lastly, equation (2.7) is Ohm's Law, which simply states that the electric current is directly proportional to the electric field.

2.1.1 Derivation of the Wave Equation

We can derive the wave equation from Maxwell's equations. From equation (2.2), we can solve for the derivative, and we obtain

$$-\frac{\partial \vec{H}}{\partial t} = \frac{1}{\mu' \mu_0} \nabla \times \vec{E}.$$

Taking the curl of both sides and using equation (2.4) gives

$$\begin{aligned} \nabla \times \frac{1}{\mu' \mu_0} \nabla \times \vec{E} &= -\frac{\partial}{\partial t} \nabla \times \vec{H} \\ &= -\frac{\partial}{\partial t} \left(\vec{J} + \frac{\partial \vec{D}}{\partial t} \right) \\ &= -\frac{\partial \vec{J}}{\partial t} - \frac{\partial^2 \vec{D}}{\partial t^2}. \end{aligned}$$

The rate of change of σ and ϵ' with time is negligible compared to that of the field vectors. Thus, we can treat σ and ϵ' as constants when differentiating with respect to time. Expressing \vec{D} and \vec{J} in terms of \vec{E} using equations (2.5) and (2.7), respectively, and multiplying through by the constant μ_0 gives

$$\nabla \times \left(\frac{1}{\mu'} \nabla \times \vec{E} \right) = -\mu_0 \sigma \frac{\partial \vec{E}}{\partial t} - \mu_0 \epsilon_0 \epsilon' \frac{\partial^2 \vec{E}}{\partial t^2}.$$

Since $\mu_0 \epsilon_0 = c^{-2}$, where c is the speed of light in a vacuum,

$$\nabla \times \left(\frac{1}{\mu'} \nabla \times \vec{E} \right) = -\mu_0 \sigma \frac{\partial \vec{E}}{\partial t} - \frac{\epsilon'}{c^2} \frac{\partial^2 \vec{E}}{\partial t^2}. \quad (2.8)$$

If μ' is isotropic and constant in space and there are no free charges ($\rho = 0$), the left-hand side of equation (2.8) can be reduced using the vector identity

$$\nabla \times (\nabla \times \vec{A}) = \nabla(\nabla \cdot \vec{A}) - \nabla^2 \vec{A}$$

to

$$\begin{aligned} \nabla \times \left(\frac{1}{\mu'} \nabla \times \vec{E} \right) &= \frac{1}{\mu'} (\nabla(\nabla \cdot \vec{E}) - \nabla^2 \vec{E}) \\ &= \frac{1}{\mu'} (\nabla(\epsilon' \epsilon_0 \rho) - \nabla^2 \vec{E}) \\ &= -\frac{1}{\mu'} \nabla^2 \vec{E}. \end{aligned}$$

So equation (2.8) becomes

$$\nabla^2 \vec{E} = \mu' \mu_0 \sigma \frac{\partial \vec{E}}{\partial t} + \frac{\epsilon' \mu'}{c^2} \frac{\partial^2 \vec{E}}{\partial t^2}.$$

Since

$$\frac{c}{\sqrt{\epsilon' \mu'}} = v,$$

where v is the speed of light in a medium, we obtain

$$\nabla^2 \vec{E} = \mu' \mu_0 \sigma \frac{\partial \vec{E}}{\partial t} + \frac{1}{v^2} \frac{\partial^2 \vec{E}}{\partial t^2}.$$

If the medium is not conductive ($\sigma = 0$), this reduces to

$$\nabla^2 \vec{E} = \frac{1}{v^2} \frac{\partial^2 \vec{E}}{\partial t^2}, \quad (2.9)$$

which is the wave equation. Equation (2.9) holds as well with \vec{E} replaced by \vec{H} .

2.1.2 Time-Harmonic Fields and the Helmholtz Equations

Our EM fields come from the application of a single-frequency harmonic wave generated by the magnetron. These fields are time-harmonic, that is, of the form

$$\vec{E} = \vec{E}_0(x, y, z)e^{i\omega t}, \\ \vec{H} = \vec{H}_0(x, y, z)e^{i\omega t},$$

where $i = \sqrt{-1}$, and $\omega = 2\pi f$ is the angular frequency.

If we plug this into equation (2.8), we obtain

$$\nabla \times \left(\frac{1}{\mu'} \nabla \times \vec{E} \right) = -i\mu_0\sigma\omega\vec{E} + \frac{\epsilon'}{c^2}\omega^2\vec{E} \\ = \left(\frac{\omega}{c} \right)^2 \left(\epsilon' - i\frac{\sigma}{\omega\epsilon_0} \right) \vec{E} \\ = \kappa_0^2 \left(\epsilon' - i\frac{\sigma}{\omega\epsilon_0} \right) \vec{E}. \quad (2.10)$$

This is the governing equation for EM fields used by FEMLAB, with $\kappa_0 = \omega/c$.

Consider the term

$$\epsilon' - i\frac{\sigma}{\omega\epsilon_0},$$

which appears on the right-hand side of equation (2.10). The imaginary part of this factor is called the dielectric loss factor, or, more simply, the loss factor, and is denoted as

$$\epsilon'' \equiv \frac{\sigma}{\omega\epsilon_0}, \quad (2.11)$$

and the entire quantity is written as the complex permittivity

$$\epsilon \equiv \epsilon' - i\epsilon''.$$

We may also write

$$\epsilon = \epsilon'(1 - i\tan\delta),$$

where

$$\tan\delta \equiv \frac{\epsilon''}{\epsilon'}$$

is called the dielectric loss tangent, or simply the loss tangent. If μ' is isotropic and constant in space, we get

$$\nabla^2\vec{E} = \left(\frac{\omega}{c} \right)^2 \mu'\epsilon\vec{E}.$$

This is the Helmholtz equation on \vec{E} , which may also be written as

$$\nabla^2\vec{E} = \left(\frac{\omega}{v} \right)^2 (1 - i\tan\delta)\vec{E}.$$

We can cancel the time-harmonic ($e^{i\omega t}$) terms and get the same equation in terms of \vec{E}_0 :

$$\nabla^2\vec{E}_0 = \left(\frac{\omega}{c} \right)^2 \mu'\epsilon\vec{E}_0.$$

We can solve directly for the \vec{H} -field by plugging the time-harmonic form directly into equation (2.2) to give

$$\vec{H}_0 = i(\mu'\mu_0\omega)^{-1}(\nabla \times \vec{E}_0). \quad (2.12)$$

Also, given the \vec{H} -field, we can find the curl of the \vec{E} -field directly from equation (2.4), which is

$$\nabla \times \vec{H}_0 = \sigma\vec{E}_0 + i\omega\epsilon'\epsilon_0\vec{E}_0 = i(\epsilon' - i\epsilon'')\omega\epsilon_0\vec{E}_0,$$

which we can write as

$$\nabla \times \vec{H}_0 = i\epsilon\epsilon_0\omega\vec{E}_0. \quad (2.13)$$

The curl equations (2.12) and (2.13) imply that $\nabla \cdot \vec{B} = 0$ and $\nabla \cdot \vec{D} = 0$, since the divergence of a curl is always zero.

Henceforth, we suppress the zero subscript and use \vec{E} and \vec{H} to refer to \vec{E}_0 and \vec{H}_0 , respectively, except where noted.

2.2 EM Boundary Conditions

Having presented the partial differential equations describing field behavior, we need to formulate the appropriate boundary conditions for our system.

Let S in Figure 2.1 denote a surface containing an interface or boundary separating two different materials. Maxwell's equations say that

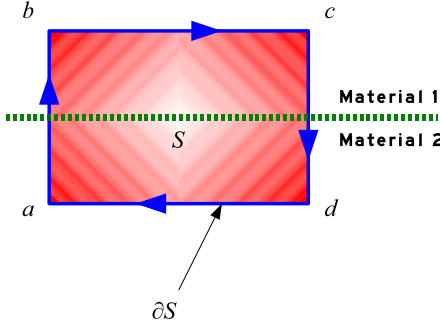


Figure 2.1. A generic surface S , with boundary ∂S and a material interface shown by the green dotted line.

$$\nabla \times \vec{E} = -\frac{\partial \vec{B}}{\partial t}.$$

An equivalent integral form is

$$\oint_{\partial S} \vec{E} \cdot d\vec{\ell} = \int_S -\frac{\partial \vec{B}}{\partial t} \cdot d\vec{s}.$$

Taking the line integral along the blue path in the figure, that is, ∂S , yields

$$\oint_{\partial S} \vec{E} \cdot d\vec{\ell} = \int_a^b \vec{E} \cdot d\vec{\ell} + \int_b^c \vec{E} \cdot d\vec{\ell} + \int_c^d \vec{E} \cdot d\vec{\ell} + \int_d^a \vec{E} \cdot d\vec{\ell}.$$

Then, if we let a approach b , and c approach d , the area of S and the length of the line segments \overline{ab} and \overline{cd} approach zero, and we have

$$\int_a^b \vec{E} \cdot d\vec{\ell} + \int_b^c \vec{E} \cdot d\vec{\ell} + \int_c^d \vec{E} \cdot d\vec{\ell} + \int_d^a \vec{E} \cdot d\vec{\ell} = \int_S -\frac{\partial \vec{B}}{\partial t} \cdot d\vec{s},$$

since we assume that $\partial \vec{B}/\partial t$ is a Riemann-integrable field. Thus,

$$\int_b^c \vec{E}_1 \cdot d\vec{\ell} + \int_d^a \vec{E}_2 \cdot d\vec{\ell} = 0,$$

where \vec{E}_1 and \vec{E}_2 are the electric fields on either side of the boundary. Now,

$$\int_b^c E_{1,\text{tang}} d\ell + \int_d^a -E_{2,\text{tang}} d\ell = 0,$$

where E_{tang} indicates the tangential component of the electric field. So

$$E_{1,\text{tang}} = E_{2,\text{tang}}. \quad (2.14)$$

Similarly,

$$H_{1,\text{tang}} = H_{2,\text{tang}}. \quad (2.15)$$

There are two types of boundary conditions associated with our system. The first is the boundary between two dielectrics (between elements of a heterogeneous load, for instance). The second is the boundary between a conductor (the waveguide) and a dielectric (the load).

2.2.1 Dielectric-Dielectric Boundary Conditions

From equations (2.14) and (2.15), the tangential components of the \vec{E} - and \vec{H} -fields are continuous across an interface. In particular, on the interface separating two dielectrics, we have

$$(\vec{E}_1 - \vec{E}_2) \times \hat{n} = \vec{0} \quad (2.16)$$

and

$$(\vec{H}_1 - \vec{H}_2) \times \hat{n} = \vec{0}. \quad (2.17)$$

Here, \hat{n} is a unit vector normal to the boundary.

2.2.2 Conductor-Dielectric Boundary Conditions

In a perfect conductor, $\vec{E} = \vec{0}$, so equation (2.16) implies that the tangential component of the \vec{E} -field of the dielectric is zero at a conducting boundary:

$$\vec{E} \times \hat{n} = \vec{0}.$$

We also need a boundary condition for the \vec{H} -field at the conductor-dielectric interface.

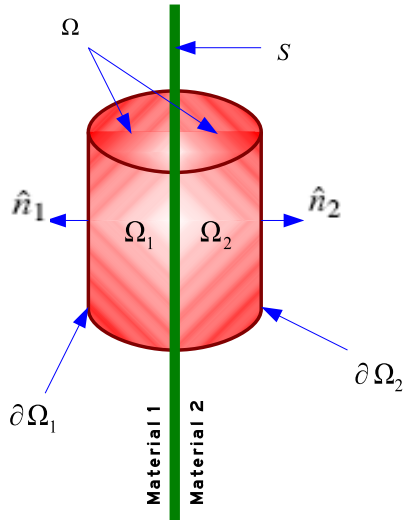


Figure 2.2. A typical material interface, shown in 3D. Here, Ω is the volumetric domain bounded by $\partial\Omega$, with subdomains Ω_1 and Ω_2 bounded by $\partial\Omega_1$ and $\partial\Omega_2$, respectively, and S denotes the material interface.

Consider Figure 2.2, where the region Ω contains an interface S separating two different materials occupying Ω_1 and Ω_2 such that $S = \partial\Omega_1 \cap \partial\Omega_2$. Let \hat{n}_1 and \hat{n}_2 be outward unit normal vectors for $\partial\Omega_1$ and $\partial\Omega_2$, respectively. The Divergence Theorem and equation (2.3) give

$$\int_{\Omega} \nabla \cdot \vec{B} dV = \int_{\partial\Omega} \vec{B} \cdot \hat{n} dS = 0.$$

In particular, we have

$$\int_{\partial\Omega_1} \vec{B} \cdot \hat{n}_1 dS + \int_{\partial\Omega_2} \vec{B} \cdot \hat{n}_2 dS = 0.$$

If we let Ω collapse such that $\partial\Omega_1 \rightarrow S$ and $\partial\Omega_2 \rightarrow S$, then

$$\int_S \vec{B}_1 \cdot \hat{n}_1 dS + \int_S \vec{B}_2 \cdot \hat{n}_2 dS = 0.$$

Since $\hat{n}_1 = -\hat{n}_2$ on S , one has

$$\int_S \vec{B}_1 \cdot \hat{n} dS - \int_S \vec{B}_2 \cdot \hat{n} dS = 0.$$

The initial region Ω was chosen arbitrarily, so we can conclude that

$$\vec{B}_1 \cdot \hat{n} = \vec{B}_2 \cdot \hat{n}$$

on the interface of two materials.

Let $\vec{B}_1 \cdot \hat{n}$ represent the normal component of \vec{B} on the conductor side of the boundary. Since $\vec{E} = \vec{0}$ inside a conductor, equation (2.2) says that there is no time-variation in the \vec{B} -field. So the normal component of the \vec{B} -field, and hence the \vec{H} -field, in the dielectric medium is zero at the interface with the conductor:

$$\vec{H} \cdot \hat{n} = 0. \quad (2.18)$$

2.2.3 Input Port Boundary Condition

At the input port, the boundary condition is that a traveling EM wave passing through the boundary will pass through it without reflection. To represent this, FEMLAB uses the numerical boundary condition

$$\hat{n} \times (\nabla \times \vec{E}) - i\kappa_n \hat{n} \times (\vec{E} \times \hat{n}) = -2i\kappa_n \hat{n} \times (\vec{E}_I \times \hat{n}), \quad (2.19)$$

where κ_n is the propagation constant (wavenumber) in the direction given by \hat{n} , and \vec{E}_I is the incident field on the boundary, which is of the form

$$\vec{E}_I = \vec{E}_{\text{tang}} e^{i(\kappa_n \hat{n} \cdot \vec{r})},$$

where $\vec{r} = \langle x, y, z \rangle$ is the position vector. For example, the boundary on which we will be using this condition is parallel to the $+z$ -axis, so \vec{E}_I is of the form

$$\vec{E}_I = \vec{E}_{\text{tang}} e^{i\kappa_z z}.$$

Any wave of the above form traveling through this boundary having the same value of κ_n will experience no reflection at the boundary. The respective condition on the \vec{H} -field is not used in this project and is not stated.

2.3 Energy Considerations

The energy flux carried by an electromagnetic wave is given by the Poynting vector

$$\vec{S} = \frac{1}{\mu' \mu_0} \vec{E} \times \vec{B} = \vec{E} \times \vec{H}.$$

The Poynting vector points in the direction of wave propagation and has magnitude equal to the power per unit area passing through a surface normal to it. [2]

It is the case that Poynting vectors on either side of a boundary may not be equal, since only the tangential components of \vec{E} and \vec{H} are required to be continuous across the material interface, as stated in equations (2.16) and (2.17). Thus, there is a loss or gain of energy. Generally, waves incident on an interface may be reflected or refracted, so not all waves hitting the boundary may pass through. Also, some energy will be absorbed by a dielectric and turned to heat if it is a lossy dielectric; this will be discussed further in Chapter 3.

2.4 Exact Solution for an Empty Waveguide

We consider a waveguide of infinite length along the $+z$ -axis and constant cross-section, placed in a vacuum:

$$\epsilon' = \mu' = 1, \quad \sigma = 0.$$

We follow the method of solution given in [2]. Start with a time-harmonic solution $\psi(x, y, z, t)$ to the scalar wave equation

$$\nabla^2 \psi = \frac{1}{c^2} \frac{\partial^2 \psi}{\partial t^2},$$

and note that given a unit vector \hat{a} , any solution of the form

$$\vec{E} = \nabla \times \psi \hat{a}$$

or

$$\vec{E} = \nabla \times \nabla \times \psi \hat{a}$$

is a solution to the vector wave equation (2.9) and satisfies the divergence condition. Note that $\vec{E} = \psi \hat{a}$ solves the vector wave equation but may not have zero divergence. For time-harmonic waves,

$$\nabla \times \nabla \times \nabla \times \psi \hat{a} = C(\nabla \times \psi \hat{a})$$

where C is a constant, so higher-order curls are redundant.

The wave will be periodic along the $+z$ -axis as well as in time, so we take

$$\psi = \phi(x, y) e^{i(\omega t - \kappa_z z)}, \quad (2.20)$$

and take $\hat{a} = \hat{k}$, the unit vector in the $+z$ direction. Taking $\vec{E} = \nabla \times \psi \hat{k}$ gives us an \vec{E} -field of the form (omitting the calculation)

$$E_x = \frac{\partial \phi}{\partial y} e^{i(\omega t - \kappa_z z)}, \quad (2.21)$$

$$E_y = -\frac{\partial \phi}{\partial x} e^{i(\omega t - \kappa_z z)}, \quad (2.22)$$

$$E_z = 0. \quad (2.23)$$

Using the curl equation for \vec{E} , equation (2.12), we obtain the components of \vec{H} :

$$\begin{aligned} H_x &= -\frac{\kappa_z}{\omega \mu_0} E_y, \\ H_y &= \frac{\kappa_z}{\omega \mu_0} E_x, \\ H_z &= -\frac{i}{\omega \mu_0} \left(\frac{\partial^2 \phi}{\partial x^2} + \frac{\partial^2 \phi}{\partial y^2} \right) e^{i(\omega t - \kappa_z z)}. \end{aligned}$$

Waves of this form are called transverse electric (TE) waves, since the \vec{E} -field is transverse (perpendicular) to the direction of propagation.

The other class of solutions can be obtained by taking $\vec{H} = \nabla \times \psi \hat{k}$, which is equivalent to taking $\vec{E} = \nabla \times \nabla \times \psi \hat{k}$. These are called transverse magnetic (TM) waves, and have the form

$$\begin{aligned} H_x &= \frac{\partial \phi}{\partial y} e^{i(\omega t - \kappa_z z)}, \\ H_y &= -\frac{\partial \phi}{\partial x} e^{i(\omega t - \kappa_z z)}, \\ H_z &= 0, \end{aligned}$$

and by equation (2.13),

$$\begin{aligned} E_x &= \frac{\kappa_z}{\omega \epsilon_0} H_y, \\ E_y &= -\frac{\kappa_z}{\omega \epsilon_0} H_x, \\ E_z &= \frac{i}{\omega \epsilon_0} \left(\frac{\partial^2 \phi}{\partial x^2} + \frac{\partial^2 \phi}{\partial y^2} \right) e^{i(\omega t - \kappa_z z)}. \end{aligned}$$

If the transverse Laplacian vanishes, that is, if

$$\frac{\partial^2 \phi}{\partial x^2} + \frac{\partial^2 \phi}{\partial y^2} = 0,$$

these two classes are redundant, and the wave is called a transverse electromagnetic (TEM) wave. Plane waves are a type of TEM wave. However, in general, the Laplacian does not vanish, and in fact will never vanish with a simple cylindrical or rectangular waveguide.

Our question now reduces to finding ϕ . If we plug $\psi = \phi(x, y)e^{i(\omega t - \kappa_z z)}$ into the scalar wave equation, the derivatives with respect to z and t can be taken explicitly, leaving a scalar Helmholtz equation for ϕ :

$$\frac{\partial^2 \phi}{\partial x^2} + \frac{\partial^2 \phi}{\partial y^2} + \kappa_c^2 \phi = 0, \quad (2.24)$$

where

$$\kappa_c^2 = \frac{\omega^2}{c^2} - \kappa_z^2,$$

with κ_c taking on discrete values according to the waveguide geometry, as we shall show later. In order for waves to propagate and not decay, we require that $\kappa_z \in \mathbb{R}$ in equation (2.20). So

$$\kappa_z^2 = \frac{\omega^2}{c^2} - \kappa_c^2 \geq 0.$$

Solving this gives us

$$\omega_c \geq c\kappa_c.$$

So there is a frequency f_c , called the cutoff frequency, below which no wave can propagate without attenuation. It is given by

$$f_c = \frac{\omega_c}{2\pi} = \frac{c\kappa_c}{2\pi}.$$

We must now address the geometry of the waveguide. For our purposes, we will only consider a waveguide of rectangular cross-section, with width $a > 0$ in the $+x$ -direction and height $b < a$ with $b > 0$ in the $+y$ -direction.

The general solution to the Helmholtz equation (2.24) is an arbitrary sum of terms of the form

$$\phi(x, y) = A \cos(\kappa_x x - \chi_x) \cos(\kappa_y y - \chi_y), \quad (2.25)$$

where

$$\kappa_x^2 + \kappa_y^2 = \kappa_c^2$$

and χ_x and χ_y are constants which determine the phase of the cosine terms.

Boundary conditions at the edges of the waveguide are that the tangential components of \vec{E} and normal components of \vec{H} must vanish. In our rectangular waveguide, this means that $E_x = 0$ at $y = 0$ and $y = b$, $E_y = 0$ at $x = 0$ and $x = a$, $H_x = 0$ at $x = 0$ and $x = a$, and $H_y = 0$ at $y = 0$ and $y = b$. Considering TE waves first, requiring equations (2.21) through (2.23) to satisfy these boundary conditions with ϕ of the form given by equation (2.25) tells us $\chi_x = \chi_y = 0$ and that κ_x and κ_y , the wavenumbers in the $+x$ - and $+y$ -directions, respectively, take on discrete values given by

$$\kappa_x = \frac{l\pi}{a}, \quad \kappa_y = \frac{m\pi}{b}, \quad (2.26)$$

where $l \in \mathbb{N} \cup \{0\}$ and $m \in \mathbb{N} \cup \{0\}$. Each l - m pair defines a TE mode, which is denoted TE_{lm} .

Explicitly, the TE modes are given by

$$\begin{aligned} E_x &= -A \frac{m\pi}{b} \cos\left(\frac{l\pi x}{a}\right) \cos\left(\frac{m\pi y}{b}\right) e^{i(\omega t - \kappa_z z)}, \\ E_y &= A \frac{l\pi}{a} \sin\left(\frac{l\pi x}{a}\right) \cos\left(\frac{m\pi y}{b}\right) e^{i(\omega t - \kappa_z z)}, \\ E_z &= 0, \\ H_x &= -A \frac{\kappa_z}{\omega \mu_0} \frac{l\pi}{a} \sin\left(\frac{l\pi x}{a}\right) \cos\left(\frac{m\pi y}{b}\right) e^{i(\omega t - \kappa_z z)}, \\ H_y &= -A \frac{\kappa_z}{\omega \mu_0} \frac{m\pi}{b} \cos\left(\frac{l\pi x}{a}\right) \cos\left(\frac{m\pi y}{b}\right) e^{i(\omega t - \kappa_z z)}, \\ H_z &= iA \frac{\pi^2}{\omega \mu_0} \left(\frac{l^2}{a^2} + \frac{m^2}{b^2} \right) \cos\left(\frac{l\pi x}{a}\right) \cos\left(\frac{m\pi y}{b}\right) e^{i(\omega t - \kappa_z z)}. \end{aligned}$$

For TM waves, requiring the boundary conditions hold gives us the same conditions on κ_x and κ_y as in equation (2.26), and that $\chi_x = \chi_y = \pi/2$ (which will result in some cosines becoming sines and *vice versa*). Again, each l - m pair defines a TM mode, which is denoted TM_{lm} . Explicitly, the TM modes are given by

$$\begin{aligned} H_x &= A \frac{m\pi}{b} \sin\left(\frac{l\pi x}{a}\right) \cos\left(\frac{m\pi y}{b}\right) e^{i(\omega t - \kappa_z z)}, \\ H_y &= -A \frac{l\pi}{a} \cos\left(\frac{l\pi x}{a}\right) \sin\left(\frac{m\pi y}{b}\right) e^{i(\omega t - \kappa_z z)}, \\ H_z &= 0, \\ E_x &= -A \frac{\kappa_z}{\omega \epsilon_0} \frac{l\pi}{a} \cos\left(\frac{l\pi x}{a}\right) \sin\left(\frac{m\pi y}{b}\right) e^{i(\omega t - \kappa_z z)}, \\ E_y &= -A \frac{\kappa_z}{\omega \epsilon_0} \frac{m\pi}{b} \sin\left(\frac{l\pi x}{a}\right) \cos\left(\frac{m\pi y}{b}\right) e^{i(\omega t - \kappa_z z)}, \\ E_z &= -iA \frac{\pi^2}{\omega \epsilon_0} \left(\frac{l^2}{a^2} + \frac{m^2}{b^2} \right) \sin\left(\frac{l\pi x}{a}\right) \sin\left(\frac{m\pi y}{b}\right) e^{i(\omega t - \kappa_z z)}. \end{aligned}$$

We can find that the cutoff frequency for both TE and TM modes is given by

$$f_c = \frac{c}{2} \sqrt{\frac{l^2}{a^2} + \frac{m^2}{b^2}}. \quad (2.27)$$

Two modes with the same cutoff frequency are referred to as degenerate. In a rectangular waveguide, TE and TM modes with $l = m$ are degenerate. For a particular waveguide, the mode with the lowest cutoff frequency is called the dominant mode. For example, for a waveguide with dimensions $a = 0.248$ m, $b = 0.124$ m designed for 915 MHz microwaves, the dominant mode is TE_{10} . The explicit equations for the fields in a rectangular waveguide resonating on the TE_{10} mode are:

$$E_x = 0, \quad (2.28)$$

$$E_y = A \frac{\pi}{a} \sin\left(\frac{\pi x}{a}\right) e^{i(\omega t - \kappa_z z)}, \quad (2.29)$$

$$E_z = 0, \quad (2.30)$$

$$H_x = -A \frac{\kappa_z \pi}{\omega \mu_0 a} \sin\left(\frac{\pi x}{a}\right) e^{i(\omega t - \kappa_z z)}, \quad (2.31)$$

$$H_y = 0, \quad (2.32)$$

$$H_z = iA \frac{\pi^2}{\omega \mu_0 a^2} \cos\left(\frac{\pi x}{a}\right) e^{i(\omega t - \kappa_z z)}. \quad (2.33)$$

2.5 Power of a TE_{10} Mode

The Poynting vector for a pure TE_{10} mode wave, as given in equations (2.28) through (2.33), is

$$\begin{aligned} \vec{S} &= \vec{E} \times \vec{H} \\ &= \left\langle \frac{i\pi^3 A^2}{a^3 \omega \mu_0} \sin\left(\frac{\pi x}{a}\right) \cos\left(\frac{\pi x}{a}\right), 0, \frac{\pi^2 A^2 \kappa_z}{a^2 \omega \mu_0} \sin^2\left(\frac{\pi x}{a}\right) \right\rangle e^{2i(\omega t - \kappa_z z)}. \end{aligned}$$

So the power of a wave passing through a cross-sectional surface S of the waveguide parallel to the $+z$ -axis, with width a in the $+x$ -direction and height b in the $+y$ -direction, is

$$\begin{aligned} P &= \iint_S \vec{S} \cdot d\vec{s} = \int_0^b \int_0^a \vec{S} \cdot \hat{k} dx dy \\ &= \int_0^b \int_0^a \frac{\pi^2 A^2 \kappa_z}{a^2 \omega \mu_0} \sin^2\left(\frac{\pi x}{a}\right) e^{2i(\omega t - \kappa_z z)} dx dy \\ &= \frac{\pi^2 A^2 b}{2a} \frac{\kappa_z}{\omega \mu_0} e^{2i(\omega t - \kappa_z z)}. \end{aligned}$$

In this equation, we note that

$$\frac{\omega\mu_0}{\kappa_z} = Z_{\text{TE}},$$

where Z_{TE} is called the impedance.

We want the real part of the time-harmonic term, time-averaged:

$$\text{Re} \left(e^{2i(\omega t - \kappa_z z)} \right) = \cos^2(\omega t - \kappa_z z).$$

The time-average of $\cos^2(\omega t - \kappa_z z)$, holding z constant, is $1/2$, so the time-averaged power is

$$P = \frac{\pi^2 A^2 b}{4aZ_{\text{TE}}}.$$

Solving for A gives

$$A = \frac{2}{\pi} \sqrt{\frac{a}{b} P Z_{\text{TE}}}.$$

This can be plugged back into the equations of a TE_{10} mode to give a wave which has time-averaged power P at $z = 0$. If a wave is generated by a magnetron of power output P , the wave in an empty waveguide will have time-averaged power P .

The equations for the incident \vec{E} -field \vec{E}_I in Section 2.2.3 is therefore

$$E_{I,x} = 0, \quad (2.34)$$

$$E_{I,y} = \frac{2}{a} \sqrt{\frac{a}{b} P Z_{\text{TE}}} \sin\left(\frac{\pi x}{a}\right), \quad (2.35)$$

$$E_{I,z} = 0, \quad (2.36)$$

where P is the power supplied by the magnetron, and $\kappa_z = \kappa_n$ from equation (2.19). Note that due to reflection, the power through a surface within a waveguide which is not infinitely long and empty may not equal P .

Chapter 3

Heat Diffusion

Heat transfer within a medium is the second of the two major physical processes that heat materials inside a microwave oven. In this section, we describe mathematically how this process works, formulate the three-dimensional heat equation, and derive the necessary boundary conditions. We conclude this chapter with a listing of the entire system of partial differential equations and their associated boundary conditions.

3.1 Formulation of the Heat Equation

We begin with Fourier's Law of Conduction from which we find the total heat flux. Next, we find the rate of change in total heat inside the body or load. Then, we apply the Law of Conservation of Energy to arrive at the heat equation without internal heat sources. Finally, we extend this equation to account for internal heat sources.

3.1.1 Fourier's Law of Conduction

Fourier's Law of Conduction says that the rate at which heat flows across a surface is directly proportional to the temperature gradient across that surface:

$$\vec{q} = -K\nabla T, \quad (3.1)$$

where \vec{q} is the heat flux vector, which points in the direction of greatest temperature decrease. Here $T = T(x, y, z, t)$ is the temperature and K is the thermal conductivity of the material, which is non-negative; $K = 0$ signifies no heat flow. The negative sign on the right-hand side is necessary because the vector ∇T always points in the direction of greatest temperature increase, but heat energy always flows from regions of higher temperature to regions of lower temperature [1].

3.1.2 Heat Flow Across a Surface

Using Fourier's Law of Conduction, the rate of heat leaving a plane surface of area dS with an outward unit normal vector \hat{n} is

$$\vec{q} \cdot \hat{n} dS = -K\nabla T \cdot \hat{n} dS. \quad (3.2)$$

We find the rate at which heat flows out of an arbitrary region Ω through its boundary $\partial\Omega$ by integrating (3.2) over the surface $\partial\Omega$:

$$\iint_{\partial\Omega} -K\nabla T \cdot \hat{n} dS.$$

Now we use the Divergence Theorem (sometimes called Gauss's Theorem), which says that if \vec{F} is an arbitrary vector function, \hat{n} is the outward unit normal vector, and Ω is an arbitrary region with bounding surface $\partial\Omega$, then

$$\iint_{\partial\Omega} \vec{F} \cdot dS = \iiint_{\Omega} \operatorname{div} \vec{F} dV = \iiint_{\Omega} \nabla \cdot \vec{F} dV$$

and so the rate at which heat leaves Ω via $\partial\Omega$ is

$$\iiint_{\Omega} -\nabla \cdot (K\nabla T) dV. \quad (3.3)$$

This is one term we need in the heat equation.

3.1.3 Rate of Change of Total Heat

The specific heat capacity c_0 of a material is the amount of energy needed to raise one unit of mass of that material by one unit of temperature. Thus, the rate of change of heat energy E in a region Ω is given by

$$\frac{dE}{dt} = \iiint_{\Omega} c_0 \frac{\partial T}{\partial t} \rho dm, \quad (3.4)$$

where ρ is the mass density of the material, and dm is the mass of a small amount of that material.

3.1.4 Law of Conservation of Energy

Figure 3.1 below states the Law of Conservation of Heat Energy.

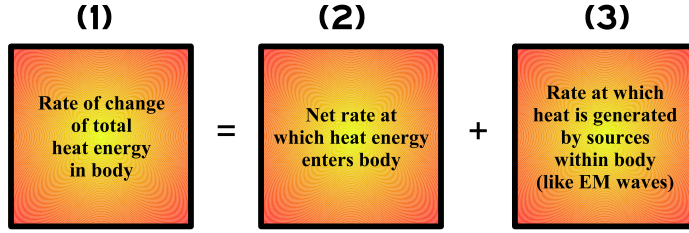


Figure 3.1. The Law of Conservation of Energy, stated in verbal form.

We have already found term (1) of Figure 3.1 as well as the negative of term (2). These correspond to equations (3.4) and (3.3), respectively. If we assume that there are no heat sources, term (3) is zero. Then we have

$$\iiint_{\Omega} \rho c_0 \frac{\partial T}{\partial t} dV = \iiint_{\Omega} \nabla \cdot (K \nabla T) dV,$$

and so

$$\iiint_{\Omega} \left(\rho c_0 \frac{\partial T}{\partial t} - \nabla \cdot (K \nabla T) \right) dV = 0.$$

Since this holds over any arbitrary region Ω , one has

$$\rho c_0 \frac{\partial T}{\partial t} - \nabla \cdot (K \nabla T) = 0.$$

When K is isotropic, we arrive at the 3D heat equation,

$$\frac{\partial T}{\partial t} = \alpha^2 \left(\frac{\partial^2 T}{\partial x^2} + \frac{\partial^2 T}{\partial y^2} + \frac{\partial^2 T}{\partial z^2} \right), \quad (3.5)$$

where

$$\alpha^2 = \frac{K}{\rho c_0}$$

is the thermal diffusivity of the material.

3.1.5 Electromagnetic Heating

The heat equation (3.5) assumes there are no internal heat sources. However, this assumption is inappropriate for our problem, since the EM waves act as an internal source of energy. So the heat equation is instead

$$\rho c_0 \frac{\partial T}{\partial t} - \nabla \cdot (K \nabla T) = Q, \quad (3.6)$$

where Q is the per volume rate of heat energy lost to the load. Specifically, the EM waves generate heat given by

$$\begin{aligned} Q &= \sigma \|\vec{E}\|^2 = \omega \epsilon_0 \epsilon''(T) \|\vec{E}\|^2 \\ &= 2\pi \epsilon_0 \epsilon''(T) f \|\vec{E}\|^2. \end{aligned} \quad (3.7)$$

The loss factor ϵ'' depends on the material and the applied wave frequency and varies with temperature.

If ϵ'' increases quickly enough with temperature, Q will increase as well, and as Q increases the temperature, there will be a feedback effect and the temperature will increase without bound. This phenomenon is called thermal runaway.

So, considering again the conservation law, the heat equation is

$$\rho c_0 \frac{\partial T}{\partial t} - \nabla \cdot (K \nabla T) - 2\pi \epsilon_0 \epsilon''(T) f \|\vec{E}\|^2 = 0. \quad (3.8)$$

3.2 Boundary Conditions

We will consider two types of boundary conditions for equation (3.8). These conditions are for the interfaces between the load and waveguide walls plus the air and load, and the interface between two materials within the load.

3.2.1 Load-Waveguide and Load-Air Interfaces

We assume that the waveguide is insulated, and also that there is no heat transfer between the air and the load. Thus, by Fourier's Law (3.1),

$$\begin{aligned} K_0 \nabla T_0 \cdot \hat{n} &= 0, \\ K_1 \nabla T_1 \cdot \hat{n} &= 0, \end{aligned}$$

where the zero subscript refers to the waveguide walls, denoted as $\partial\Omega_0$, indicating that no heat crosses the interface [1].

3.2.2 Load-Load Interface

Let S be a surface separating two different materials within the load. The net rate of heat flow per unit area out of a material across a surface is given by $-K \nabla T \cdot \hat{n}$ where \hat{n} is the unit normal to the surface pointing away from the material. So, since the net rate of heat going from material 1 to material 2 across S must equal the net rate of heat flow entering material 2 across S , we have

$$-K_1 \nabla T \cdot \hat{n}_1 = K_2 \nabla T \cdot \hat{n}_2.$$

Since $\hat{n}_2 = -\hat{n}_1$, the boundary condition at a dielectric-dielectric interface is

$$K_1 \nabla T \cdot \hat{n} = K_2 \nabla T \cdot \hat{n}.$$

In FEMLAB, this is called a continuity boundary condition, and applies only when we have a heterogeneous load.

3.3 Governing Equations

We will consider here a simple example consisting of a waveguide of arbitrary cross-section with some mashed potatoes inside it, and a single pea sitting inside the mashed potatoes as illustrated in Figure 3.2. Regions Ω_1 and Ω_2 are the load and Ω_0 is the air.

Table 3.3 shows the governing set of partial differential equations and boundary conditions for our system.

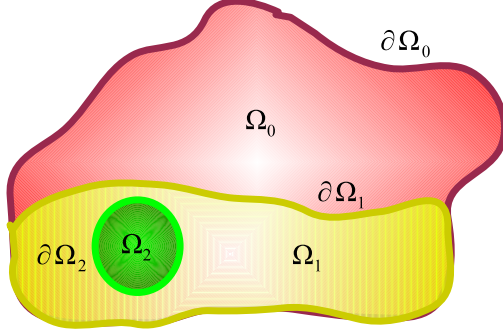


Figure 3.2. A heterogeneous load inside a waveguide. Region Ω_1 represents the mashed potatoes, while Ω_2 is a single pea inside the mashed potatoes.

Governing Equations			
EM	$\nabla \times \left(\frac{1}{\mu'} \nabla \times \vec{E} \right) = \frac{\omega^2}{c} (\epsilon' - i\epsilon'') \vec{E}$		
Heat	$\rho c_0 \frac{\partial T}{\partial t} - \nabla \cdot (K \nabla T) = 2\pi \epsilon_0 \epsilon'' f \ \vec{E}\ ^2$		
Boundary Conditions			
	$\partial\Omega_0$	$\partial\Omega_1$	$\partial\Omega_2$
EM	$\vec{E} \times \hat{n} = \vec{0}$	$(\vec{E}_0 - \vec{E}_1) \times \hat{n} = \vec{0}$	$(\vec{E}_1 - \vec{E}_2) \times \hat{n} = \vec{0}$
Heat	$K \nabla T \cdot \hat{n} = 0$	$K \nabla T \cdot \hat{n} = 0$	$K_1 \nabla T \cdot \hat{n} - K_2 \nabla T \cdot \hat{n} = 0$

Table 3.1. The system of governing equations and boundary conditions for Figure 3.2.

Chapter 4

Implementation in FEMLAB

In the previous two chapters, we discussed and formulated a mathematical model for our problem. The second step is to implement this model in FEMLAB¹, a multiphysics modeling tool. In this chapter, we begin by discussing how to implement our governing equations listed in Section 3.3, as well as the boundary conditions. We also discuss material constants, such as thermal conductivity K and the loss factor ϵ'' as they relate to FEMLAB. Later in the chapter we discuss mesh size phenomena, FEMLAB's linear solvers, and how to vary the magnetron power output in time.

4.1 Common Elements of Our Models

We consider a WR975 waveguide, i.e. one that is 248×124 mm in cross-section:

$$a = 0.248 \text{ m},$$

$$b = 0.124 \text{ m},$$

$$\frac{b}{a} = \frac{1}{2}.$$

Our waveguide is closed at one end, with EM waves coming in the other. We consider a fixed frequency $f = 915$ MHz. At this frequency, WR975 waveguides can only support a TE₁₀ mode, as shown in Table 4.1. We always assume our materials have no magnetic losses ($\mu' = 1$); this holds for almost all dielectrics.

4.2 Layout of the Model in FEMLAB

The first (fairly trivial) step in the implementation of our model in FEMLAB is to draw out each of the subdomains. Our layout is shown in Figure 4.1. We have two subdomains: one for the air (subdomain 1) and the other for the

¹All information in this chapter and the next pertains to FEMLAB 3.1i, the latest version of the software as of July 2005. However, as of June 2006, Comsol, Inc. has renamed the software to COMSOL MULTIPHYSICS™, meaning that the precise implementation procedures described here may differ slightly in the new version. Thus, whenever we refer to FEMLAB, we refer to COMSOL MULTIPHYSICS™.

Mode	f_c (MHz)
TE ₁₀	605
TE ₀₁	1210
TE ₁₁	1352
TE ₂₀	1210
TE ₀₂	2419
TE ₂₁	1711
TE ₁₂	2494
TE ₂₂	2705

Table 4.1. Calculated cutoff frequencies for selected TE modes in a WR975 waveguide.

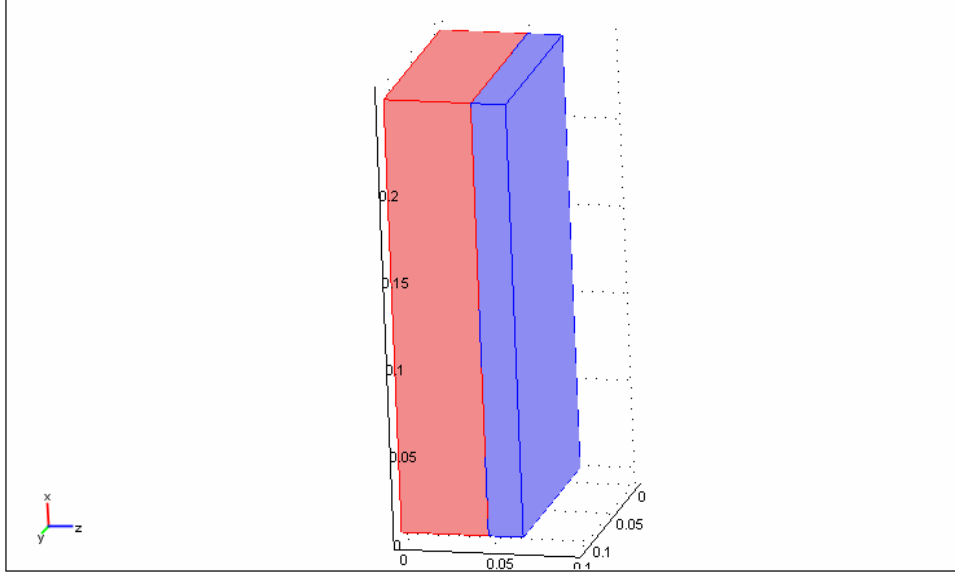


Figure 4.1. Subdomains and boundaries used for our model in FEMLAB.

homogeneous load (subdomain 2). In Figure 4.1, the air is indicated in red while the load is indicated in blue.

Each subdomain has width and height as specified in the previous section. In this case, the air has length 0.05 m while the load has length 0.02 m. The length of each subdomain will always be stated before we present results for a particular numerical experiment.²

There are 11 boundaries in our geometry. In Figures 4.4 and 4.5, boundary 3 is the input port.

4.3 Implementation of Governing Equations in FEMLAB

FEMLAB supplies both the EM and heat equations as formulated in Chapters 2 and 3 in the Electromagnetics and Heat Transfer Modules, respectively. Some names and notation in FEMLAB are different from ours, and are noted. Any setting not mentioned is left as the default. We also explain the specific geometry of the problems.

4.3.1 Electromagnetic Waves

We define constants in FEMLAB inside the **Constants** dialog box, as in Figure 4.2, where a is the width of the waveguide along the $+x$ -axis, $\lambda_{\text{amx_TE10}}$ is the wavelength (in Hz) in the $+x$ -direction of the TE_{10} mode, k_x_{TE10} is the wavenumber in the $+x$ -direction (from equation (2.26)) of the TE_{10} mode, and Pow is the power output of the magnetron (W), which can be changed to suit the problem. We also change the scalar variable nu_wch , which we have referred to as the frequency f , to be $915\text{e}6$.

We now configure each of the subdomains in the **Subdomain Settings** dialog box. Each subdomain obeys equation (2.10). Relative permittivity $\epsilon_r = \epsilon'$ and electrical conductivity σ vary per material; we discuss the exact nature of these values in Section 4.4. FEMLAB uses electrical conductivity σ instead of the loss factor ϵ'' , but these are related by the formula

$$\sigma = 2\pi f \epsilon_0 \epsilon'',$$

which is simply equation (2.11). We take σ to account for all losses given by ϵ'' . Also, $\mu_r = \mu' = 1$. See Figure 4.3.

The boundary conditions on each boundary between the waveguide and the outside is the perfect electric conductor condition given in Section 2.2.2. The internal boundary condition between the load and air within the waveguide is the continuity condition given by equation (2.16). At the incoming port, the boundary condition is given in Section 2.2.3 with applied field given by equations (2.34) through (2.36); specifically, we create the boundary expressions in the

²Although these subdomain lengths are highly impractical, they are chosen in this manner in order to save computational time.

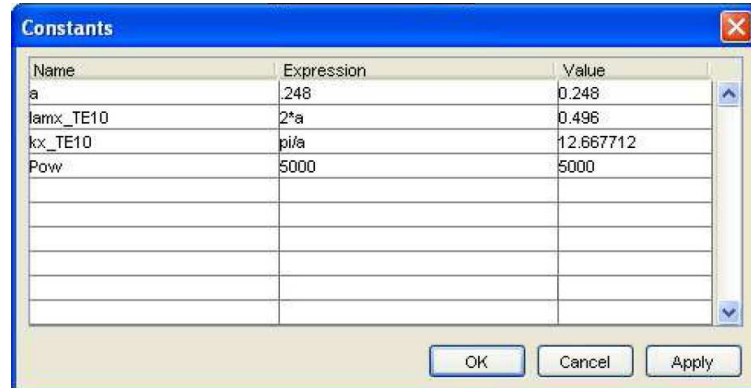


Figure 4.2. The **Constants** dialog box in FEMLAB.

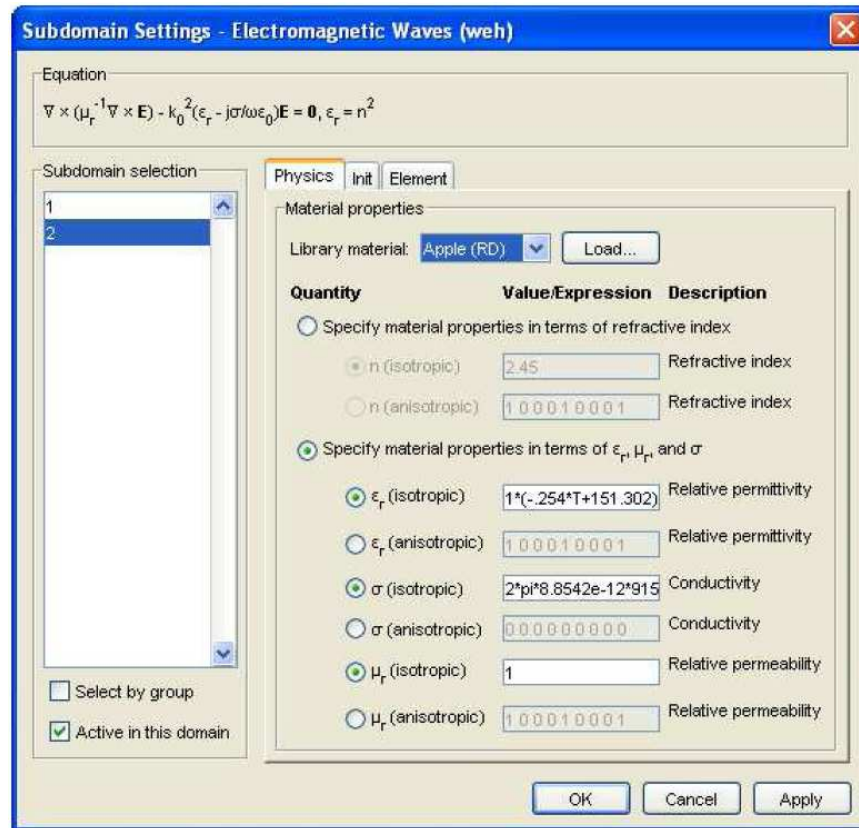


Figure 4.3. The **Subdomain Settings** dialog box in the Electromagnetics Module of FEMLAB. The governing EM equation is shown at the top, along with the subdomain to which it applies (Subdomain 2 is the load in this case, which is solid red delicious apple). Dielectric and magnetic properties are entered here as well.

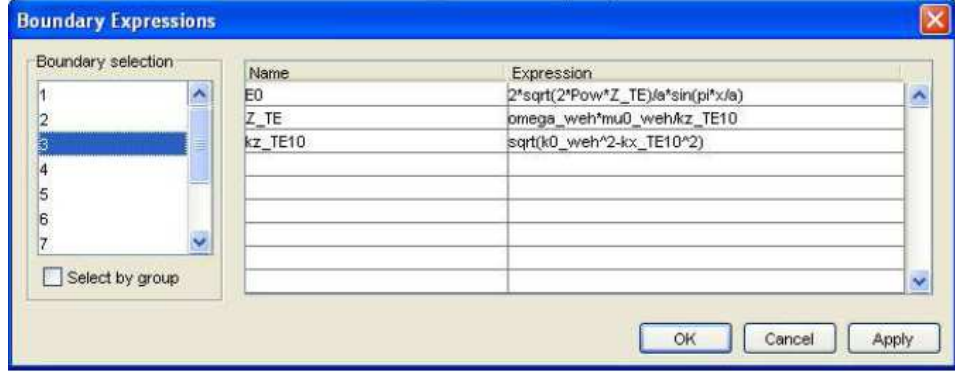


Figure 4.4. The **Boundary Expressions** dialog box in the Electromagnetics Module in FEMLAB.

Boundary Expressions dialog box as in Figure 4.4, where $\kappa_z_TE10 = \kappa_z$ is the wavenumber in the direction of propagation, Z_TE is the impedance, $E0 = E_{I,y}$ in equation (2.35), and in $E0$ the aspect ratio $a/b = 2$. Then, in the **Boundary Settings** dialog box, we set the boundary condition to **Matched Boundary**, and set

$$\mathbf{E}_0 = \vec{E}_I = \langle 0, E_0, 0 \rangle$$

and we set the propagation constant β to be κ_z_TE10 . See Figure 4.5. Using the port condition and setting the field by hand would be equivalent. We cannot use the built-in rectangular modes because the port condition would normalize the wave to a power of 1 W.

4.3.2 Heat Transfer

The temperature distribution on the subdomains that contain the load is determined by equation (3.8). In the **Subdomain Settings** dialog box within the Heat Transfer Module (see Figure 4.6), the heat source Q is set to be $Q_{av,weh}$, which is equation (3.7), time-averaged. The constants of thermal properties are mass density ρ , specific heat capacity $C = c_0$, and thermal conductivity $k = K$, and vary per material. We assume that the boundary between the air and the load is completely insulating, so we can disable heat transfer in the air. Initial temperature in both is set at 20°C .

In the **Boundary Settings** dialog box within the Heat Transfer Module in FEMLAB, all boundaries between the load and the waveguide are set to **Thermal Insulation**, as given in Section 3.2.1. The internal boundary between the load and air is set to **Continuity** (Section 3.2.2), which is equivalent to thermal insulation since there is no heat transfer in the air. Boundaries within the load are set to **Continuity**.

4.4 Material Constants

In the **Subdomain Settings** dialog boxes in both the Electromagnetics and Heat Transfer Modules, dielectric and thermal properties of the load are needed. We have collected an index of properties of various materials for use in our models. This index consists of values for ρ , c_0 , K , ϵ' , and ϵ'' . We take ρ , c_0 , and K to be constant, and $\epsilon'(T)$ and $\epsilon''(T)$ to be functions of temperature. To obtain the functions for ϵ' and ϵ'' , we collected experimental data from various literature sources. We obtained data listed at several different temperatures between 0°C and 100°C , since this is the temperature range in which we are interested. We then plotted the data on a chart, and in most cases we used a linear fit from standard linear regression techniques. Tap water is an exception to this rule, since a more complex function approximation is directly available.

The table of values for several foods is given in Appendix A.

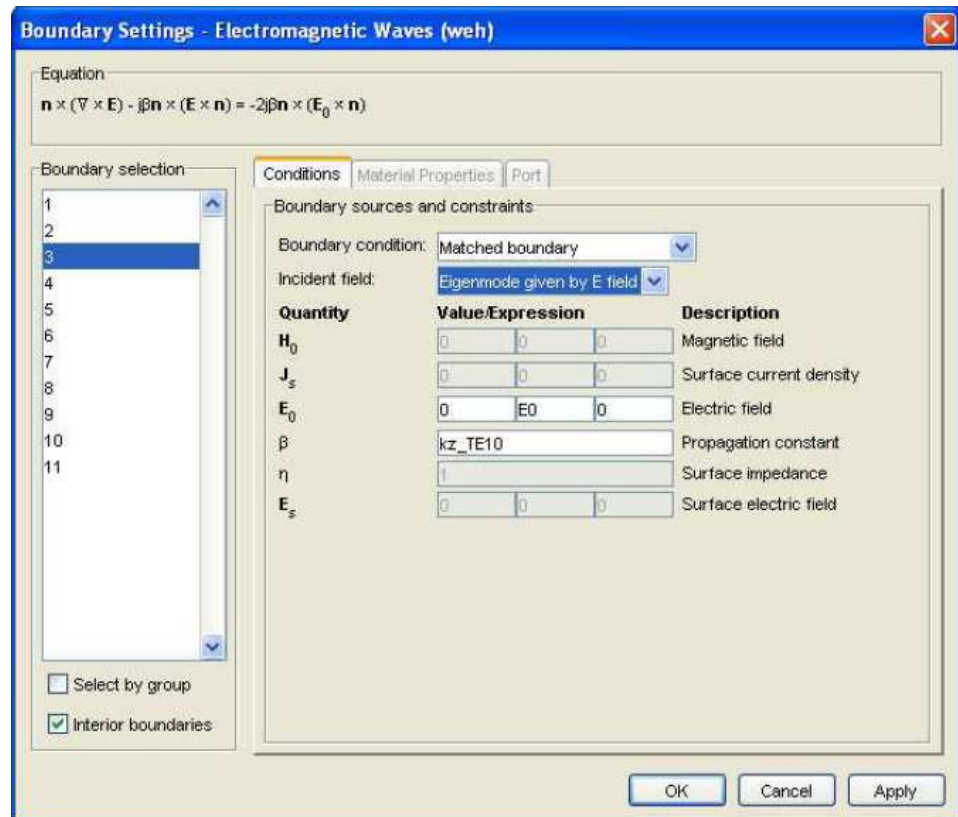


Figure 4.5. FEMLAB's **Boundary Settings** dialog box for EM waves, located in the Electromagnetics Module. In this box, we enter values for \mathbf{E}_0 and β . Boundary 3 is the input port.

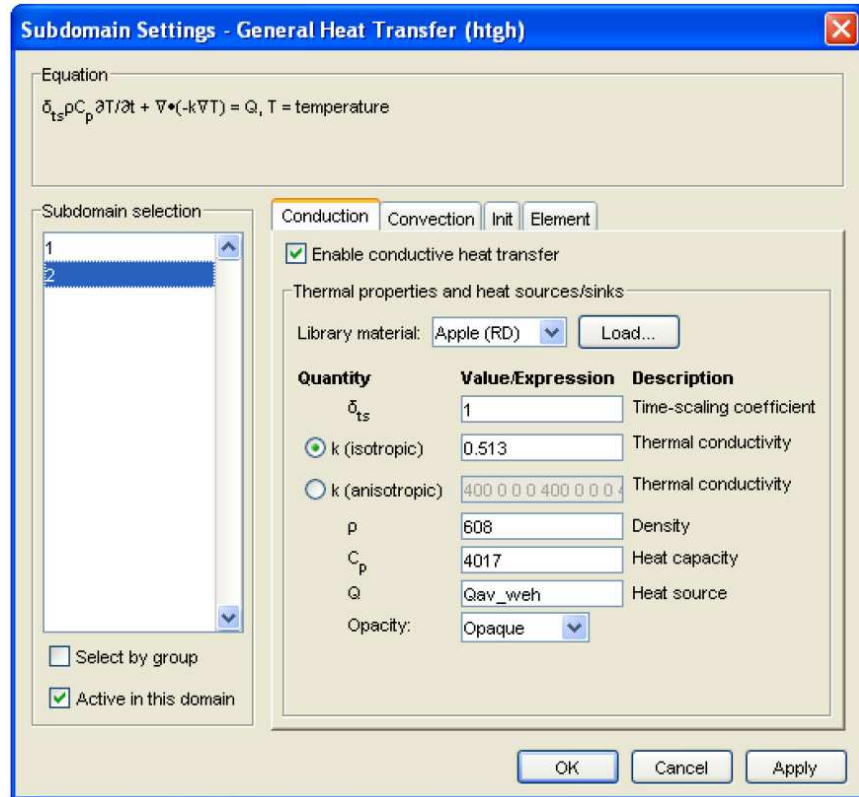


Figure 4.6. The **Subdomain Settings** dialog box, located in the Heat Transfer Module. The heat equation is shown at the top of the box, along with the subdomain to which it applies (in this case it is subdomain 2, which is the load). Thermal properties are entered in this box. The time-scaling coefficient $\delta_{ts} = 1$ for every numerical experiment we conduct.

4.5 Solving the Model

In solving the model, we must make sure that we have accurate results, and that what we propose to do is not too computationally intensive.

4.5.1 The Nyquist Criterion

The Nyquist Criterion says that when numerically solving any harmonic function, to obtain accurate numerical results, it is necessary for the maximum grid element size s_{\max} to be less than half the wavelength:

$$s_{\max} < \frac{\lambda}{2} = \frac{c}{2f\sqrt{\epsilon' \mu'}}$$

where λ is the wavelength, f is the frequency of the wave, c is the speed of light in a vacuum, ϵ' is the dielectric constant, and μ' is the relative permeability. [5]

For example, in free space, the requirement is $s_{\max} < 0.163$ m. In a material where $\epsilon' = 79$, which is near that of water and many other food materials, $s_{\max} < 0.018$ m.

4.5.2 Choice of Linear System Solver

FEMLAB implements five different time-dependent linear system solvers to solve the linear system that the finite element method creates. It can be found by inspecting the equation system in FEMLAB that our coupled system does not result in a symmetric linear system, so the only solvers we may possibly use are the two direct solvers, called UMFPACK (Unsymmetric Multi-Frontal Package) and SPOOLES (Sparse Object-Oriented Linear Equations Solver), and the iterative solver GMRES (Generalized Minimum Residual) with one of the following preconditioners: Incomplete LU, Geometric Multigrid, and Algebraic Multigrid.

According to the FEMLAB documentation, UMFPACK is the default solver. Its main advantage is that it is fairly efficient in terms of both computational time and accuracy. However, it is also very memory-intensive; after running a few experiments, we found that UMFPACK quickly runs out of memory when solving the coupled model with smaller mesh sizes. Therefore, SPOOLES is the preferable direct solver, since our memory resources are limited, even though we may end up sacrificing some accuracy of the results.

We now turn to the iterative solver, GMRES. This solver comes with the three preconditioners listed above. Consulting FEMLAB's documentation, it is critical to choose the preconditioner that is appropriate for our problem. The Algebraic Multigrid preconditioner works poorly on vector PDEs and does not support complex numbers, so it is unsuitable for our model. The Geometric Multigrid preconditioner works by using a series of refined meshes. On the initial mesh, Geometric Multigrid starts out by using a direct solver, most likely SPOOLES, so GMRES with the Geometric Multigrid preconditioner is only a better choice than SPOOLES if we are trying to achieve a level of refinement on which SPOOLES runs out of memory. Geometric Multigrid, even then, is poorly suited to the system.

We performed some more careful analysis on the Incomplete LU preconditioner. This preconditioner works by approximating an LU factorization of the system matrix \mathbf{A} . It performs this approximation during the Gaussian elimination stage of the LU factorization by changing certain elements of \mathbf{A} to zero. This mapping of elements $a_{i,j}$ of \mathbf{A} is as follows:

$$a_{i,j} \mapsto \begin{cases} 0 & \text{if } |a_{i,j}| < d, \\ a_{i,j} & \text{if } |a_{i,j}| \geq d, \end{cases}$$

where d is called the drop tolerance, which we can specify. Values for d typically range from as high as 0.2 to as low as 10^{-5} . It is important to understand where we should set the drop tolerance if we desire accurate results without using excessive amounts of memory. The FEMLAB documentation states that there are several advantages and disadvantages of setting either a high or low drop tolerance. These are listed in Table 4.2.

We ran the GMRES solver using the Incomplete LU conditioner with

$$d = 0.2, 0.1, 0.05, 0.02, 0.01, 0.005, 0.002, 0.001, 5 \times 10^{-4}, 10^{-4}, \text{ and } 10^{-5},$$

using the model parameters listed in Table 4.3.

	<i>Advantages</i>	<i>Disadvantages</i>
<i>d small</i>	More accurate results Fewer iterations needed	Increased memory usage Increased preconditioning time
<i>d large</i>	Decreased memory usage Decreased preconditioning time	Less accurate May not converge

Table 4.2. Pros and cons of small and large values of d for the GMRES solver with the Incomplete LU preconditioner.

Waveguide Dimensions	Air Tap water	$0.248 \times 0.124 \times 0.01$ m $0.248 \times 0.124 \times 0.01$ m
Maximum Element Size	Air Tap water	$0.02 \text{ m} < s_{\max} = 0.163 \text{ m}$ $0.014 \text{ m} < s_{\max} = 0.018 \text{ m}$
T_{init}	Air Tap water	20°C 20°C
$\epsilon'(T)$	Air Tap water ³	N/A $-0.285T + 85$
Coupling		Full 2-way
$P(t)$		5000 W
t		$t \in [0, 15]$ s, 1 s increments

Table 4.3. Parameters used in experimenting with drop tolerance values.

We measured memory usage and computational time. The results are shown in Figures 4.7 and 4.8.

As the drop tolerance decreases, the solution time remains little changed at first, but then increases dramatically if the drop tolerance becomes too small. This is problematic since we want to minimize solution time. However, Figure 4.8 reveals another problem. As drop tolerance decreases, memory usage increases, dramatically so as the drop tolerance becomes very small.⁴ Because of our limited memory resources on our computers, this is also problematic. A third issue is convergence of the iterations. In our analysis, we found that if $d \geq 0.01$, the iterations do not converge to a solution. According to FEMLAB's documentation on this preconditioner, the optimal way to use this solver and preconditioner is to set the drop tolerance so that it is only slightly less than the threshold for convergence. In our case, this threshold lies somewhere between 0.005 and 0.01.

Our results show that GMRES with the Incomplete LU preconditioner has long run times, runs out of memory, and is thus poorly suited for our system. Therefore, we will use the SPOOLES solver in our numerical experiments.

³This function is a linear approximation for the actual function, which is given in Appendix A. An explanation of why this function is used is given in Section 5.3.

⁴It is important to point out that memory usage readings are taken from FEMLAB's status bar, shown at the bottom right-hand corner of FEMLAB's window. These readings should not be confused with the total system memory usage while FEMLAB's solver is running, as these numbers will be substantially higher than those shown in the chart. The general trend of memory usage versus drop tolerance values, however, remains unchanged.

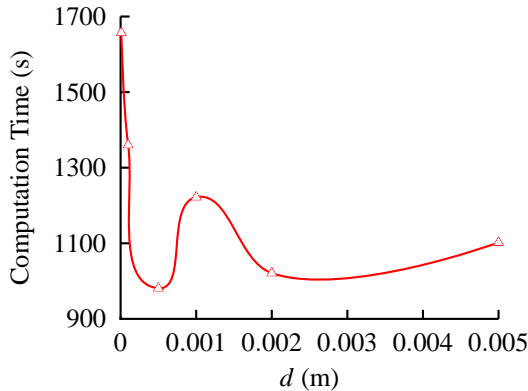


Figure 4.7. Solve time vs. d .

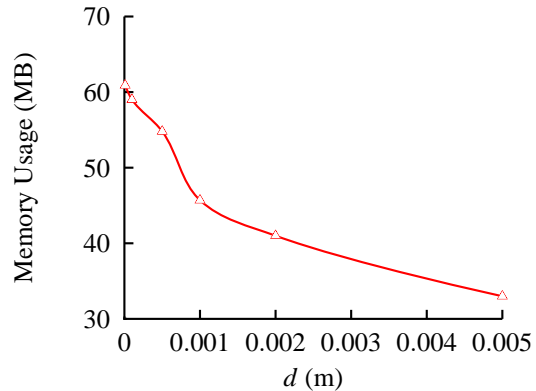


Figure 4.8. Memory usage vs. d .

Chapter 5

Numerical Experiments and Results

We have arrived at the most critical part of the project: running the experiments using FEMLAB aiming to fulfill the goals listed in Chapter 1. In this chapter, we explain the experiments we perform, what we expect to find by running these experiments, the system parameters used, and finally, the results and our analysis.

5.1 Accuracy of FEMLAB's EM Field Solution

We first want to ensure that FEMLAB gives accurate solutions for the EM field. We compare FEMLAB's solution for $\|\vec{E}\|$, the norm of the \vec{E} -field, against that of *QuickWave-3D*. *QuickWave-3D* is used by microwave engineers and researchers to simulate EM wave propagation, and is trusted to give accurate results. The waveguide in both models is as described in Table 4.3, with a tap water load. Heating is not considered here.

As can be seen from Figures 5.1 and 5.2, the results match very well. However, as $z \rightarrow 0$, *QuickWave-3D*'s solution approaches zero; this is a known problem of the software, and does not affect the rest of the \vec{E} -field. FEMLAB's solution is slightly uneven, which is due to the nonregular discretization, and not exactly symmetric about the center line, which is due to the nonsymmetric discretization. If the grid size became smaller, the \vec{E} -field profile would approach *QuickWave-3D*'s solution.

5.2 Role of Thermal Diffusion

We want to know if heat diffusion plays a major role in microwave heating. If not, then simply modeling the EM fields would suffice.

We run the fully coupled model with and without heat diffusion. To simulate the absence of diffusion, we set $K = 0$; otherwise we leave K to be the actual value for the material. We run this experiment on four materials. Again, the model parameters are as given in Table 4.3. We summarize the results in Figure 5.3 as well as Tables 5.1 and 5.2.

The minimum temperatures T_{\min} are clearly nonsensical for all materials except baked potato for $K > 0$, since $T_{\text{init}} = 20^\circ\text{C}$ inside the load.¹ Values for T_{\max} are consistently higher in the case where $K = 0$, especially so for baked potato. The heating profiles for baked potato with and without diffusion are shown in Figure 5.3. The percentage decline in temperature ranges between the cases $K = 0$ and $K > 0$ ranges from 26% to 38%, suggesting that accounting for heat diffusion will drastically reduce discrepancies in the temperature distribution; heating would thus be more uniform.

Values for average temperatures \bar{T} are nearly identical except for those with raw turkey as the load. It is possible that the effects of diffusion cause the average temperatures to be slightly different because of the change in ϵ' and ϵ'' with temperature, but it is not possible to tell from this data if that is true.

Overall, these results indicate that the role of diffusion is certainly important for some materials.

¹As of July 2006, there are several students in the REU program at WPI who are investigating this issue. Early indications are that the error may be FEMLAB-generated.

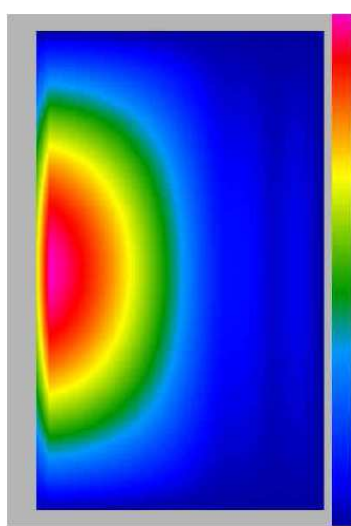


Figure 5.1. QuickWave-3D's solution for $\|\vec{E}\|$.

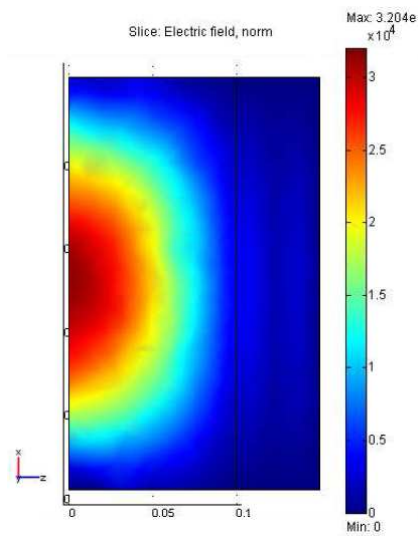


Figure 5.2. FEMLAB's solution for $\|\vec{E}\|$.

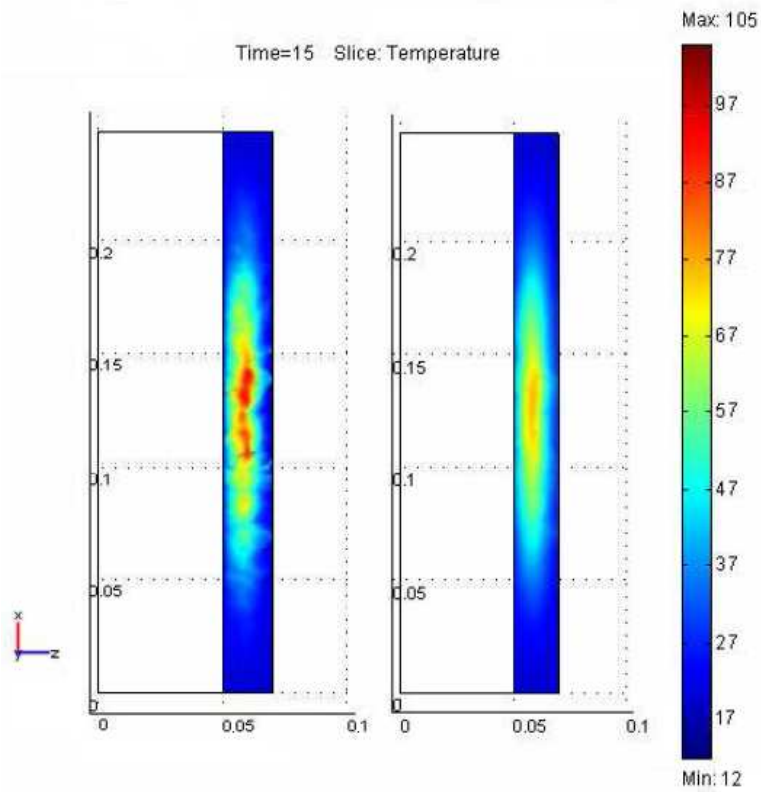


Figure 5.3. Heating profiles for baked potato, with $K = 0$ (left) and with $K = 0.641$ (right).

No Diffusion: $K = 0$						
Load	T_{init} (°C)	T_{\min} (°C)	ΔT (°C)	% Chg.	Comparison with $K > 0$	
					ΔT_{\min} (°C)	$\Delta(\%) \text{ Chg.}$
Baked potato	20	10.593	-9.407	-3.211	-9.421	-3.216
Raw turkey	20	11.511	-8.489	-2.897	-6.285	-2.145
Apple (RD)	20	14.548	-5.452	-1.861	-4.061	-1.386
Tap water	20	19.083	-0.917	-0.313	-0.709	-0.242
Load	T_{init} (°C)	T_{\max} (°C)	ΔT (°C)	% Chg.	Comparison with $K > 0$	
					ΔT_{\max} (°C)	$\Delta(\%) \text{ Chg.}$
Baked potato	20	104.933	84.933	28.987	26.114	8.912
Raw turkey	20	63.152	43.152	14.728	6.922	2.363
Apple (RD)	20	48.622	28.622	9.769	6.186	2.112
Tap water	20	26.135	6.135	2.094	1.448	0.494
Load	T_{init} (°C)	\bar{T} (°C)	ΔT (°C)	% Chg.	Comparison with $K > 0$	
					$\Delta \bar{T}$ (°C)	$\Delta(\%) \text{ Chg.}$
Baked potato	20	36.915	16.915	5.773	0.457	0.156
Raw turkey	20	40.222	20.222	6.902	10.352	3.533
Apple (RD)	20	24.077	4.077	1.391	0.008	0.002
Tap water	20	20.979	0.979	0.334	-0.002	-0.001
With Diffusion: $K > 0$						
Load	T_{init} (°C)	T_{\min} (°C)	ΔT (°C)	% Chg.	Comparison with $K = 0$	
					ΔT_{\min} (°C)	$\Delta(\%) \text{ Chg.}$
Baked potato	20	20.014	0.014	0.005	9.421	3.216
Raw turkey	20	17.796	-2.204	-0.752	6.285	2.145
Apple (RD)	20	18.609	-1.391	-0.475	4.061	1.386
Tap water	20	19.792	-0.208	-0.071	0.709	0.242
Load	T_{init} (°C)	T_{\max} (°C)	ΔT (°C)	% Chg.	Comparison with $K = 0$	
					ΔT_{\max} (°C)	$\Delta(\%) \text{ Chg.}$
Baked potato	20	78.819	58.819	20.075	-26.114	-8.912
Raw turkey	20	56.230	36.230	12.365	-6.922	-2.363
Apple (RD)	20	42.436	22.436	7.657	-6.186	-2.112
Tap water	20	24.687	4.687	1.600	-1.448	-0.494
Load	T_{init} (°C)	\bar{T} (°C)	ΔT (°C)	% Chg.	Comparison with $K = 0$	
					$\Delta \bar{T}$ (°C)	$\Delta(\%) \text{ Chg.}$
Baked potato	20	36.458	16.458	5.617	-0.457	-0.156
Raw turkey	20	29.870	9.870	3.369	-10.352	-3.533
Apple (RD)	20	24.069	4.069	1.389	-0.008	-0.002
Tap water	20	20.981	0.981	0.335	0.002	0.001

Table 5.1. Results for simulations without diffusion ($K = 0$) and with diffusion ($K > 0$).

Temperature Ranges With and Without Diffusion				
Load	$K = 0$ (°C)	$K > 0$ (°C)	Chg. (°C)	% Chg.
Baked potato	94.340	58.805	-35.535	-37.667
Raw turkey	51.641	38.434	-13.207	-25.575
Apple (RD)	34.074	23.827	-10.247	-30.073
Tap water	7.052	4.895	-2.157	-30.587

Table 5.2. Temperature range data for $K = 0$ and $K > 0$.

Waveguide Dimensions	Air Tap water	$0.248 \times 0.124 \times 0.01$ m $0.248 \times 0.124 \times 0.01$ m
Maximum Element Size	Air Tap water	$0.01 \text{ m} < s_{\max} = 0.163 \text{ m}$ $0.01 \text{ m} < s_{\max} = 0.018 \text{ m}$
T_{init}	Air Tap water	20°C 20°C
$\epsilon'(T)$	Air Tap water	N/A $-0.285T + 85$
$\epsilon''(T)$	Air Tap water	N/A $-3.68 \times 10^{-6}T^3 + 1.03 \times 10^{-3}T^2 - 0.0947T + 5.6$
Coupling		1-way
Solver		SPOOLES
$P(t)$		5000 W
t		$t \in [0, 60]$ s, 5 s increments

Table 5.3. Model parameters used in the one-way coupling vs. two-way coupling experiment.

T ($^\circ\text{C}$)	ϵ'		ϵ''	t (s)
	Nonlinear	Linear		
0	∞	85.000	5.600	12
10	96.199	82.150	4.752	10
20	84.896	79.300	4.089	9
30	78.283	76.450	3.589	8
40	73.592	73.600	3.225	7
50	69.952	70.750	2.980	6
60	66.979	67.900	2.831	5
70	64.466	65.050	2.756	5
80	62.288	62.200	2.732	6
90	60.367	59.350	2.737	7
100	58.649	56.500	2.750	10

Table 5.4. Elapsed time for tap water to boil for set values of ϵ' and ϵ'' with given constant values of T .

5.3 Temperature Dependence of ϵ' and ϵ''

In the following set of experiments, we address the need for two-way coupling of our system. Up until this point, we have assumed that the dielectric constant ϵ' and the dielectric loss factor ϵ'' vary with temperature. We say that our model is two-way coupled because the solution to the governing EM equation depends on the solution to the heat equation and *vice versa*.

But is the variation of ϵ' and ϵ'' with temperature crucial to the model? Can we just use a constant value for these instead? If we used constant values for these material properties, our system would be one-way coupled, since the solution to the governing EM equation would be independent of the solution to the heat equation. The advantage of one-way coupling is computational time: a one-way coupled model would take drastically less time to solve than a two-way coupled model.

Our approach to this experiment is as follows: we use the temperature-dependent functions for ϵ' and ϵ'' , and substitute set values for the temperature T . Since we are only interested in the temperature range from 0°C to 100°C , we will start by letting $T = 0$, and then run 10 additional trials in 10°C increments until we reach 100°C . We measure the elapsed time until $T_{\max} = 100^\circ\text{C}$.

In FEMLAB, the procedure is the following: in the **Solver Parameters** dialog box, we set the solver type to **Stationary Linear**, since in one-way coupling, the EM component is time-independent. We shall use the SPOOLES solver. In the **Solver Manager** dialog box under the **Solve For** and **Output** tabs, we highlight only the **Electromagnetic Waves** part. After this computation by FEMLAB is complete, we turn on the time-dependent solver and compute the temperature distribution using the EM result.

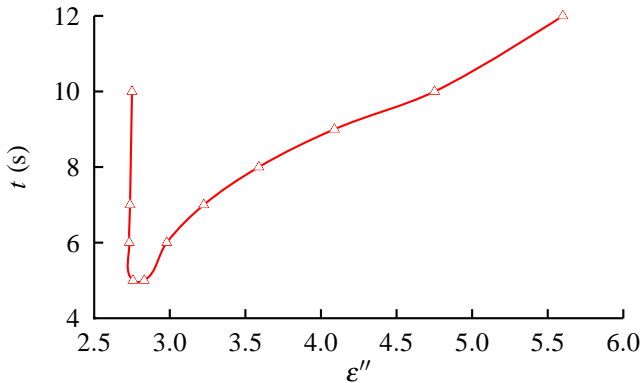


Figure 5.4. Constant values for ϵ'' cause notable variations in the time for tap water to reach 100°C.

The system parameters are shown in Table 5.3. Table 5.4 shows the values of T we used in the functions for ϵ' and ϵ'' . The function that we use for ϵ' is a linearized version of the approximating function given in Appendix A. This was necessary, otherwise we would end up taking the natural logarithm of a non-positive number when the computed tap water temperature falls below 0°C. In all cases, the computation time needed by the stationary linear solver to solve the EM portion of the model was approximately 5 s, and the time needed by the time-dependent solver ranged from 90 s to 120 s. Figure 5.4 shows the effect of varying ϵ'' on the time t to reach 100°C, and a display of FEMLAB's solution at $t = 5$ s for $T = 60$ and $T = 100$ is shown in Figure 5.5. The conclusion we draw from this chart is that there is notable variation in the time it takes for tap water to reach 100°C. This means that if two-way coupling of our system were unnecessary, we would expect there to be very little (if any) variation in these times on the chart. The fact that there is notable variation tells us that two-way coupling of our system is indeed necessary if we intend to obtain accurate results.

5.4 A Pulsing Power Source

The aim of this section is to help address the question of whether more, less, or about the same degree of heating uniformity results from having a pulsing power function or a lower, constant power function for $P(t)$. Presently, there has been much discussion about this among microwave power engineers, but no raw data to support any claims that either type of power function is better.

5.4.1 Motivation

Differences in electric field strength and heterogeneities in the load lead to nonuniform heating patterns. In other words, localized overheating (“hot spots”) and underheating are common problems in microwave thermal processing. Understanding the nature of nonuniform heating is one of the main tasks in controlling microwave thermal processing. Further, attaining heating uniformity essentially reduces to the task of controlling the behavior of hot spots.

Diffusion acts to reduce the intensity of hot spots, but while a power source is on, EM heating continues. This phenomenon sometimes overshadows the diffusion process and furthers the risk of overheating some spots. So a strategy to efficiently achieving heating uniformity is to allow for thermal relaxation. Thermal relaxation occurs when heat diffuses in the presence of no additional EM energy hitting the load.

One idea is to use a pulsed EM power source. In the time that the power source is off, the load undergoes thermal relaxation, thus reducing temperature differences within the dielectric. Here, we compare the effects of using a constant power source versus introducing a higher power pulsing source. We test the role of a pulsing source, and consequently the role of thermal relaxation, by running experiments with different types of loads and varying pulses. It is likely that depending on the initial condition imposed on the load and on the desired heating pattern, pulsing could prove either beneficial or detrimental.

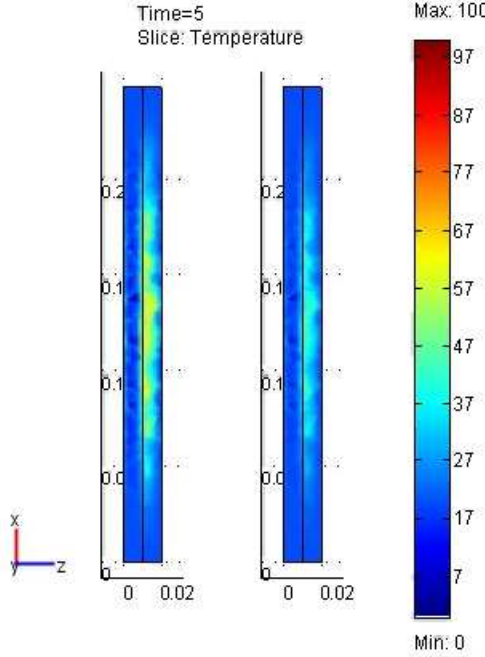


Figure 5.5. Temperature distribution inside tap water at $t = 5$, with ϵ' and ϵ'' corresponding to $T = 60$ (left) and $T = 100$ (right).

However, before we attempt to evaluate the role of pulsing at all, it is very important to ensure that we use a reasonable pulse for a given situation. Consider the pulsed power source given in Figure 5.6. Let L_1 and L_2 represent the “on” and “off” phases of the pulse, respectively. Let

$$p = L_1 + L_2$$

denote the period of the pulse and let $P(t)$ denote the power output function. The choices for L_1 , L_2 , p , and $P(t)$ vary greatly depending on the conditions of heating. For instance, if the primary constraint is on T_{\max} , we need to ensure that $P(t)$ is not too large. If the load is not as sensitive to overheating as it is to localized underheating (as in the case of thawing a piece of frozen meat), L_2 as compared with L_1 might be of utmost importance. Further, given that heat flow varies with time (temperature gradients decrease with time, thereby slowing diffusion), it makes sense to vary L_1 and L_2 with t in order to compensate for the varying rates of diffusion. It suffices to say that this problem of optimizing the pulse with respect to parameters including the ones stated is not a trivial or peripheral one; rather, optimization sits at the crux of evaluating the role of a pulsing source.

5.4.2 Implementation in FEMLAB

Suppose we have a power source that transmits pulses of duration $L_1 > 0$ at the start of every interval of duration $p \geq L_1 > 0$. The function

$$\begin{aligned} f : [0, \infty) &\rightarrow \mathbb{R}, \\ f(t) &= \sin\left(\frac{2\pi}{p}t + \chi\right) - \sin\chi \end{aligned}$$

where

$$\chi = \frac{\pi(p - 2L_1)}{2p}$$

has the following property:

$$f(t) \begin{cases} > 0 & t \in (np, np + L_1) \quad \forall n \in \mathbb{Z} \\ < 0 & t \in (np + L_1, (n+1)p) \quad \forall n \in \mathbb{Z}. \end{cases}$$

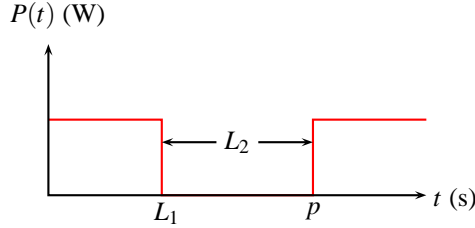


Figure 5.6. A dynamically pulsing function for $P(t)$.

So

$$P(t) = P_0 H \left(\sin \left(\frac{2\pi}{p} t + \chi \right) - \sin \chi \right)$$

where P_0 is the magnetron power output during the “on” stage and $H(t)$ is the smoothed Heaviside step function.

When using a smoothed Heaviside step function (such as one of the four that FEMLAB implements), care must be taken to make sure that $f(t) \gg 0$ so as not to be confused by the smoothing. For example, if L_1 is very small, then

$$\max_t f(t) < 1,$$

so $H(t) < 1$ during the pulse. If there is a smoothing parameter (in FEMLAB it is ε), it can be changed to make the interval over which the smoothing takes place smaller. Alternatively, the function

$$P(t) = P_0 H \left(\frac{\sin \left(\frac{2\pi}{p} t + \chi \right) - \sin \chi}{1 - \sin \chi} \right)$$

can be used, which ensures that

$$\max_t \left(\frac{\sin \left(\frac{2\pi}{p} t + \chi \right) - \sin \chi}{1 - \sin \chi} \right) = 1.$$

5.4.3 Pulsing Results

We illustrate a rather simple case to test the role of a pulsing source. Figure 5.7 shows T_{\max} at time increments of 5 s for two scenarios: a tap water load subjected to a constant power source of 5 kW, and to a pulsing power source with $P_0 = 10$ kW, $p = 10$ s, and $L = 5$ s.

In Figure 5.7, we see that at $t = 10$, $t = 20$, and $t = 30$, there is no significant difference in T_{\max} . At these times, an equal amount of power has hit the load since $t = 0$. These results tell us that while heating with constant power output produces roughly linear heating in time, a pulsing power source first heats the load at a faster rate, then at the moment the pulse is switched off, T_{\max} peaks, and then heat slowly diffuses, which in turn lowers T_{\max} . This heating pattern repeats itself every 10 s, which corresponds to the period of the pulse p .

While these results themselves do not provide any definite conclusions, we should bear in mind certain questions, such as whether increasing p would make a difference, whether changing L relative to p would make a difference (what happens as $L_1/p \rightarrow 1$?), and whether varying the load change these results. Addressing these questions is crucial to truly understanding the effects of a pulsing power source on heating patterns.

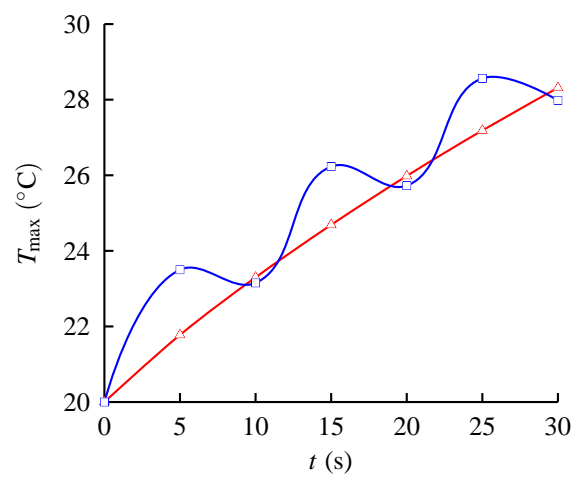


Figure 5.7. Results of T_{\max} versus t with a tap water load with $P(t)$ pulsing (blue) and $P(t)$ constant (red).

Chapter 6

Conclusions

We have developed a coupled model for microwave thermal processing and successfully implemented it in FEMLAB. This model can accommodate different geometries and loads, and simulate different microwave systems.

We have compiled a library of the available temperature-dependent material properties for various dielectrics. This library should be helpful to future researchers. Based on our computational experiments, we have found that modeling diffusion coupled with EM wave propagation is certainly essential for some materials. The degree to which diffusion is important for a material appears to be a complex relationship of its material properties. We have also performed experiments which indicate that, indeed, accounting for the temperature dependence of material properties may be necessary in modeling microwave thermal processing.

6.1 Limitations of FEMLAB

Memory issues in FEMLAB prevent us from using the grid size we desired. A maximum grid element size of approximately 8.5 mm within the load is ideal. However, on grids with a maximum element size less than 0.01 m, we began to receive out-of-memory errors from FEMLAB during the solution process.

Software specifically tailored to the problem would most likely improve our results and computational times. Much more computational work seems to be spent solving the EM wave propagation part than the heat diffusion part, so it may help to use a more efficient method for the EM wave propagation portion, such as FDTD (finite-difference time-domain), and couple that with a suitable numerical scheme for solving the heat equation.

Chapter 7

Future Work

We have provided a solid foundation for work to continue on the coupled model of microwave thermal processing. Our work here should enable researchers to approach many issues they have not been able to with previous models. We outline here some specific problems for future WPI and REU students to explore.

In particular, The Ferrite Company, Inc., currently shows interest in the following problems:

- In attaining heating uniformity in a heterogeneous load, what role do particles with a high loss factor play? What role does a low-loss medium play?
- How does varying the size of particles within a load affect the way the load is heated?

The pulse optimization problem outlined in Chapter 5 is essential to drawing any definitive conclusions about the role of pulsing. The few results we have regarding pulsing should be treated as fairly inconclusive, as we test only a few materials and scenarios here. It would be a worthwhile effort to understand and solve the optimization problem.

We would like to move the model to a more powerful computer with more memory. This would allow us to achieve more accurate results, and to consider more complicated situations.

Appendix A

Dielectric and Thermal Properties of Loads

In this appendix, we present the data collected for values of dielectric constants, loss factors, electrical conductivities, thermal conductivities, specific heat capacities, and densities. We fit our data with linear functions, with the exception of tap water. The following 33 sections contain the material properties as well as plots of the data with their approximating curves. This library contains material properties for the following dielectrics: almond [7], apple (golden delicious and red delicious) [7], baked potato [8], ceramics [7], cheese sauce [12], cherry [7], codling moth [7], cooked beef [11], cooked beef juice [11], cooked carrots, cooked ham, cooked macaroni noodles [12], cooked turkey [11], cooked turkey juice [11], cottage cheese [4], flour [7], grapefruit [7], Indian-meal moth [7], liquid whey protein mixture [12], macaroni and cheese [12], mashed potato [3], Mexican fruitfly [7], navel orange worm [7], orange [7], raw beef [11], raw turkey [11], skimmed milk powder [7], solid potato [8], tap water [6], walnut [7], and whey protein gel [12].

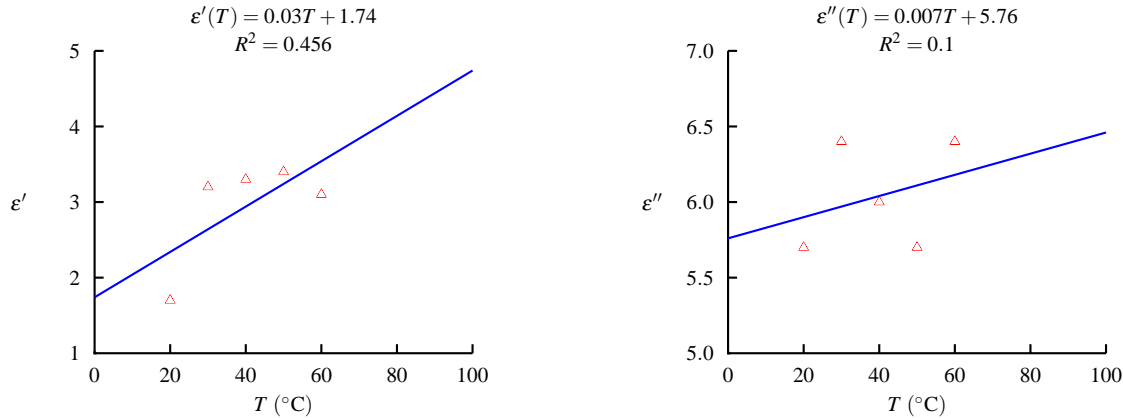
All material properties listed here are assumed to hold for $f = 915$ MHz unless explicitly stated otherwise. Values for R^2 , the relative predictive power of the model, are given where available. Although we give functions for ϵ'' here, functions for σ required by FEMLAB can easily be obtained using the formula

$$\sigma(T) = 2\pi f \epsilon_0 \epsilon''(T).$$

A.1 Almond

Values for K , c_0 , and ρ are available only for $T = 20$.

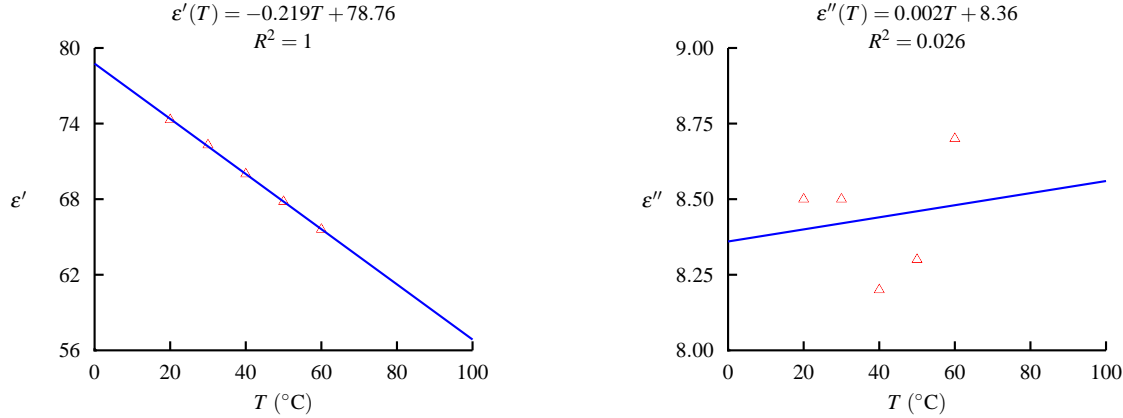
T (°C)	ϵ'	ϵ''	σ (S/m)	K (W/(m·°C))	c_0 (J/(kg·°C))	ρ (kg/m ³)
20	1.7	5.7	0.290	0.12	1170	460
30	3.2	6.4	0.326			
40	3.3	6.0	0.305			
50	3.4	5.7	0.290			
60	3.1	6.4	0.326			



A.2 Golden Delicious Apple

Values for K , c_0 , and ρ are available only for $T = 20$.

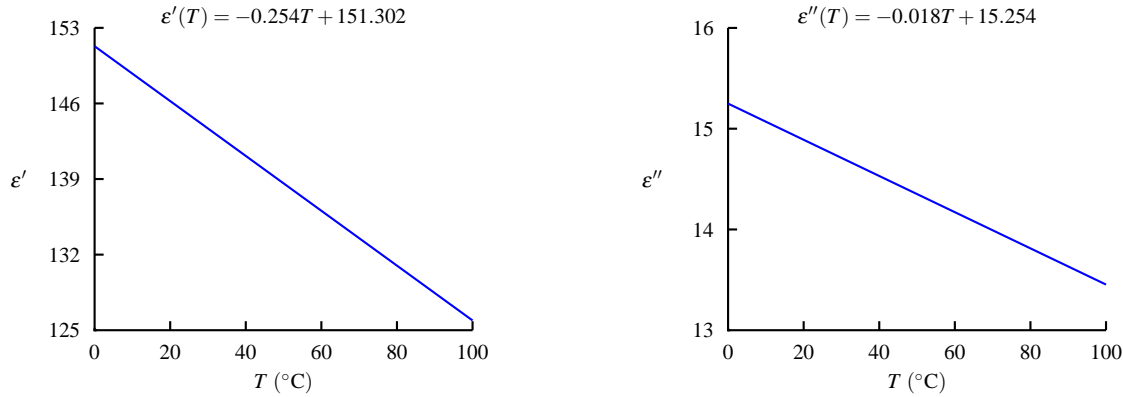
T ($^{\circ}\text{C}$)	ϵ'	ϵ''	σ (S/m)	K (W/(m \cdot $^{\circ}\text{C}$))	c_0 (J/(kg \cdot $^{\circ}\text{C}$))	ρ (kg/m 3)
20	74.3	8.5	0.433	0.447	4017	608
30	72.3	8.5	0.433			
40	70.0	8.2	0.417			
50	67.8	8.3	0.422			
60	65.6	8.7	0.443			



A.3 Red Delicious Apple

Although a function for ϵ' and ϵ'' are available here, they were found from standard linear regression techniques using data not available here. Values for ϵ' , ϵ'' , and σ at $T = 20$ were found using the given functions.

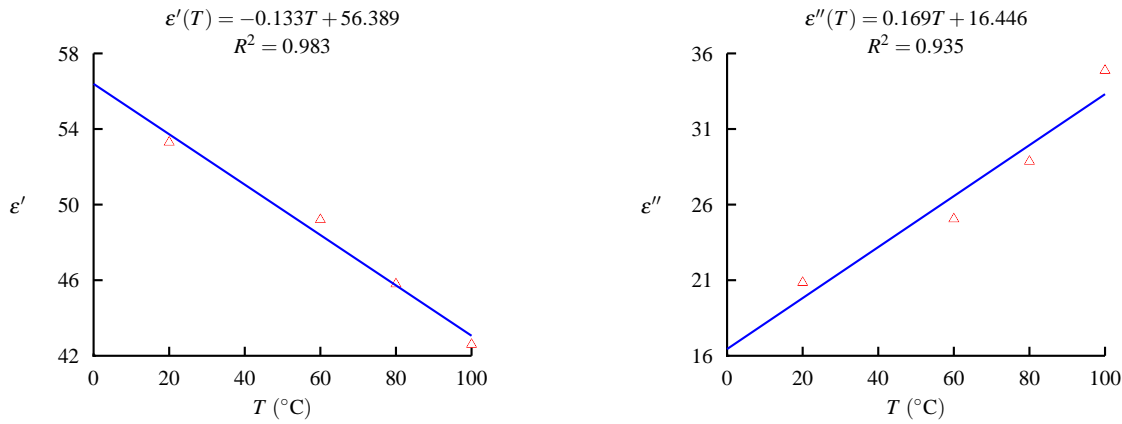
T ($^{\circ}\text{C}$)	ϵ'	ϵ''	σ (S/m)	K (W/(m \cdot $^{\circ}\text{C}$))	c_0 (J/(kg \cdot $^{\circ}\text{C}$))	ρ (kg/m 3)
20	146.2	14.9	7.443	0.513	4017	608
30						
40						
50						
60						



A.4 Baked Potato

Values for K , c_0 , and ρ are available only for $T = 20$.

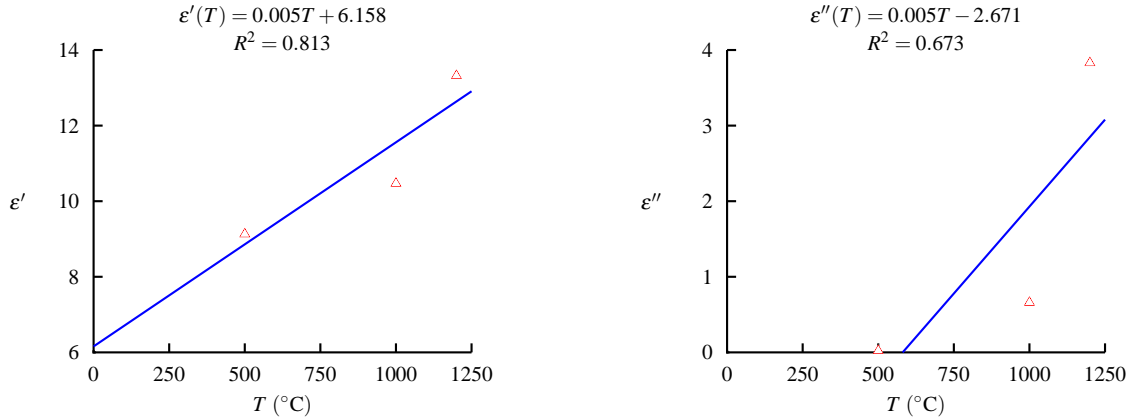
T (°C)	ϵ'	ϵ''	σ (S/m)	K (W/(m·°C))	c_0 (J/(kg·°C))	ρ (kg/m³)
20	53.3	20.844	1.061	0.641	1715	769
60	49.2	25.048	1.275			
80	45.8	28.859	1.469			
100	42.6	34.870	1.775			



A.5 Ceramic Materials

Values for K , c_0 , and ρ for this material are not available. The model should only be used for $T \geq 500$, as $\epsilon'' \geq 0$.

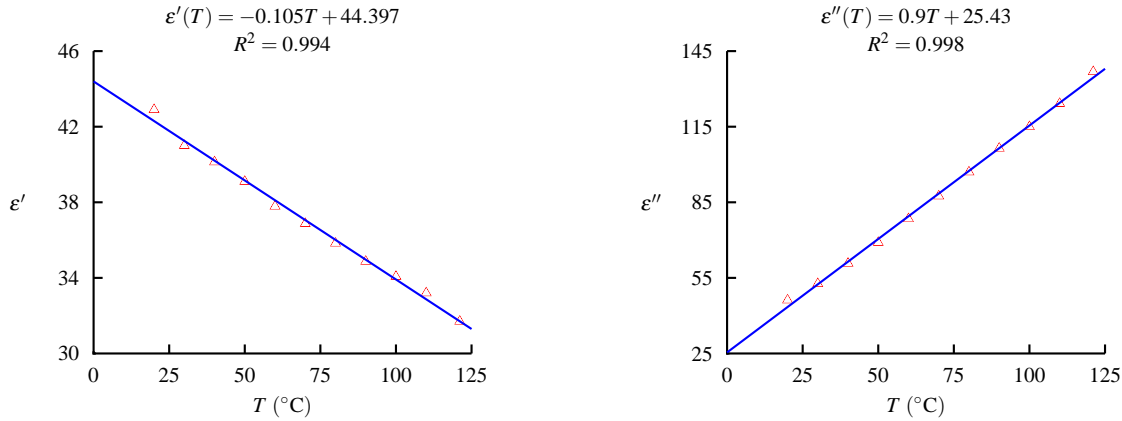
T (°C)	ϵ'	ϵ''	σ (S/m)	K (W/(m·°C))	c_0 (J/(kg·°C))	ρ (kg/m³)
500	9.13	0.022	0.001			
1000	10.47	0.660	0.034			
1200	13.32	3.830	0.195			



A.6 Cheese Sauce

Values for K , c_0 , and ρ are not available for this material.

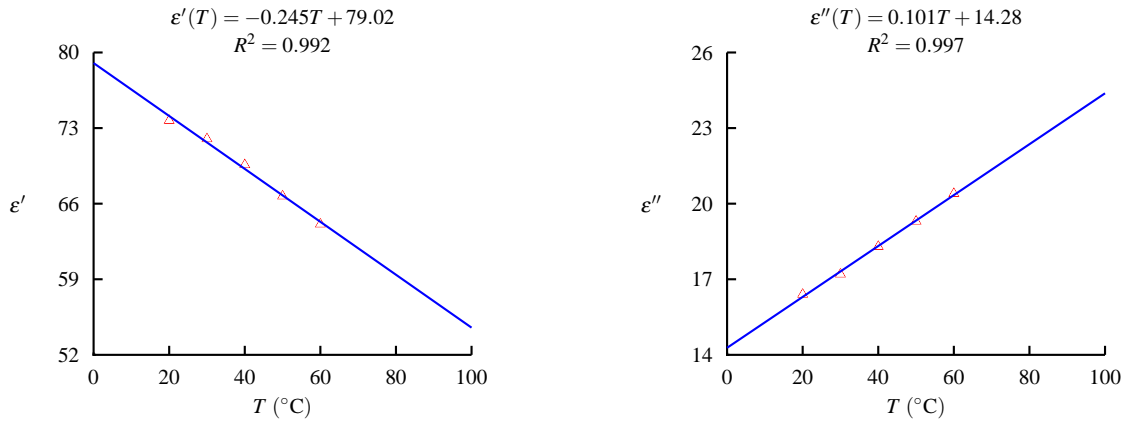
T (°C)	ϵ'	ϵ''	σ (S/m)	K (W/(m·°C))	c_0 (J/(kg·°C))	ρ (kg/m³)
20	42.90	46.17	2.350			
30	41.00	52.70	2.683			
40	40.13	60.77	3.093			
50	39.10	69.03	3.514			
60	37.87	78.43	3.992			
70	36.87	87.47	4.452			
80	35.83	97.00	4.938			
90	34.87	106.43	5.418			
100	34.07	114.97	5.852			
110	33.20	124.17	6.321			
121.1	31.70	136.80	6.963			



A.7 Cherry

Values for K , c_0 , and ρ are available only for $T = 20$.

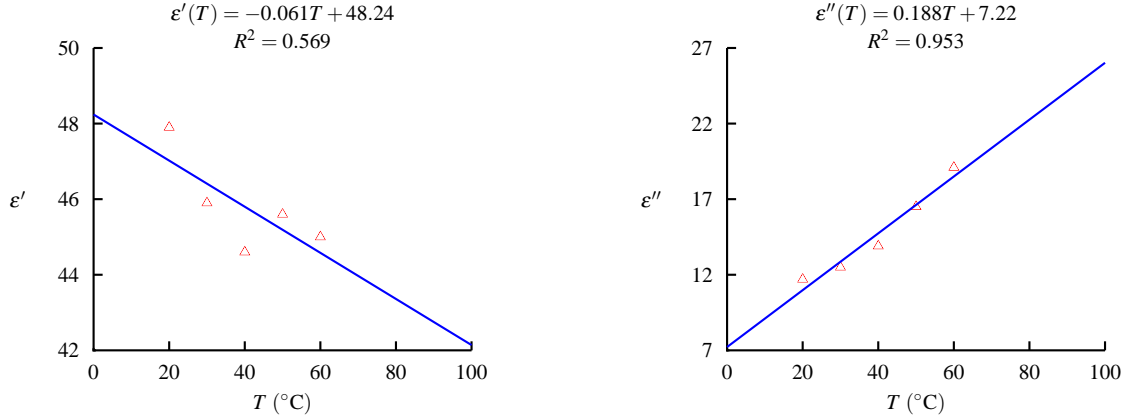
T (°C)	ϵ'	ϵ''	σ (S/m)	K (W/(m·°C))	c_0 (J/(kg·°C))	ρ (kg/m³)
20	73.7	16.4	0.835	0.553	3520	721
30	72.0	17.2	0.876			
40	69.6	18.3	0.932			
50	66.7	19.3	0.982			
60	64.1	20.4	1.038			



A.8 Codling Moth

Values for K , c_0 , and ρ are not available for this material.

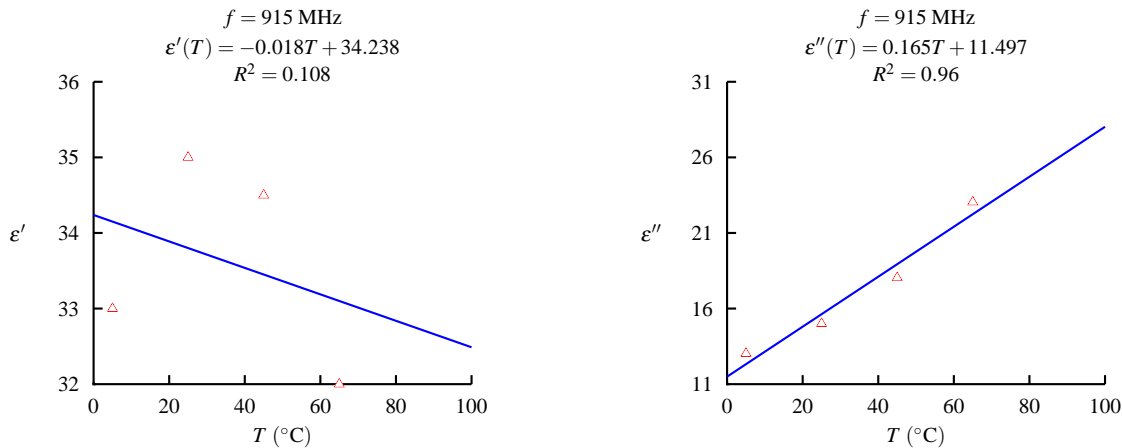
T (°C)	ϵ'	ϵ''	σ (S/m)	K (W/(m·°C))	c_0 (J/(kg·°C))	ρ (kg/m³)
20	47.9	11.7	0.596			
30	45.9	12.5	0.636			
40	44.6	13.9	0.708			
50	45.6	16.5	0.840			
60	45.0	19.1	0.972			



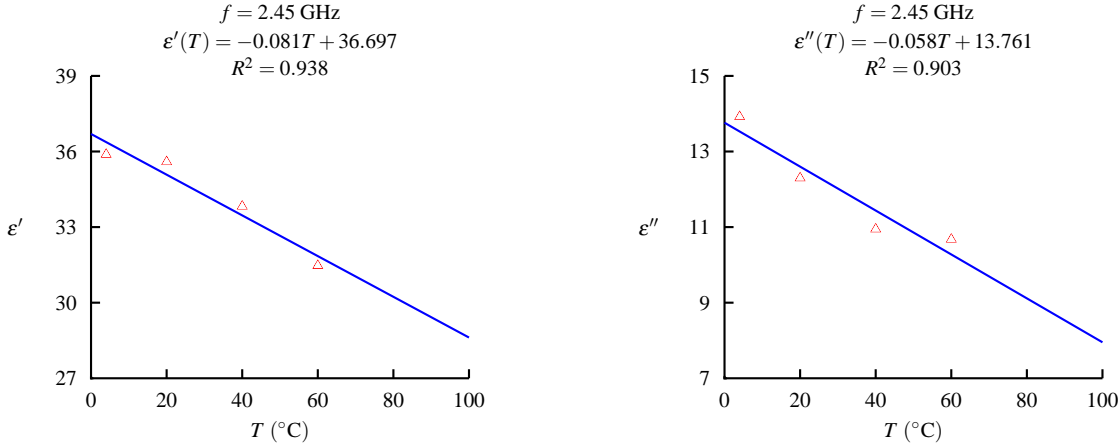
A.9 Cooked Beef

All dielectric and thermal property values given here assume 72% water content. Values for ϵ' , ϵ'' , and σ are available for both standard microwave oven frequencies. Values for K and ρ are available only for $T = 25$ for $f = 915$ MHz and for $T = 20$ for $f = 2.45$ GHz. Values given for c_0 are valid for $0 \leq T \leq 30$.

$f = 915$ MHz						
T (°C)	ϵ'	ϵ''	σ (S/m)	K (W/(m·°C))	c_0 (J/(kg·°C))	ρ (kg/m³)
5	33.0	13.025	0.663		3810	
25	35.0	15.029	0.765	0.454	3810	1070
45	34.5	18.034	0.918			
65	32.0	23.044	1.173			
$f = 2.45$ GHz						
T (°C)	ϵ'	ϵ''	σ (S/m)	K (W/(m·°C))	c_0 (J/(kg·°C))	ρ (kg/m³)
-20	5.556	0.857	0.117			
-10	6.944	1.286	0.175			
4	35.882	13.919	1.897		3810	
20	35.588	12.297	1.676	0.454	3810	1070
40	33.824	10.946	1.492			
60	31.471	10.676	1.455			



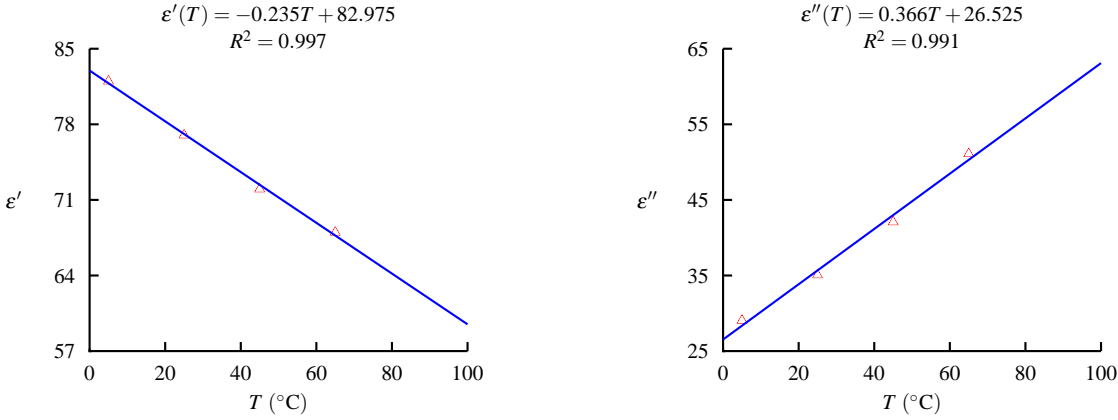
The linear fit described for ϵ' and ϵ'' for $f = 2.45$ GHz uses only data for which $T \geq 0$ due to the large change in the behavior of these functions.



A.10 Cooked Beef Juice

Values for K , c_0 , and ρ are not available for this material.

T (°C)	ϵ'	ϵ''	σ (S/m)	K (W/(m·°C))	c_0 (J/(kg·°C))	ρ (kg/m³)
5	82	29.055	1.479			
25	77	35.067	1.785			
45	72	42.080	2.142			
65	68	51.098	2.601			

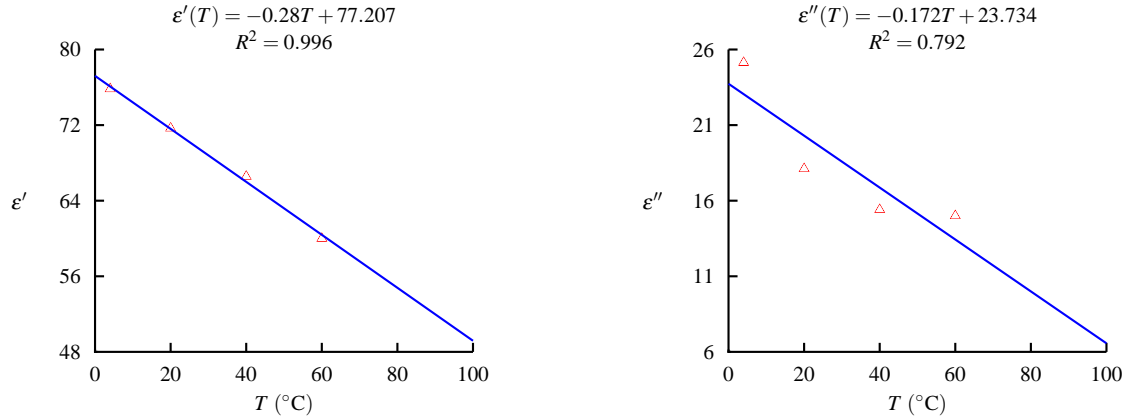


A.11 Cooked Carrots

All data listed here holds ONLY for $f = 2.45$ GHz. Values for $f = 915$ MHz are not available. Values for K , c_0 , and ρ are available only for $T = 20$.

T (°C)	ϵ'	ϵ''	σ (S/m)	K (W/(m·°C))	c_0 (J/(kg·°C))	ρ (kg/m³)
-10	5.278	0.571	0.078			
4	75.833	25.135	3.426			
20	71.667	18.108	2.468	0.564	3770	640
40	66.571	15.405	2.100			
60	60.000	15.000	2.044			

The linear fit described for ϵ' and ϵ'' uses only data for which $T \geq 0$ due to the large change in the behavior of these functions.

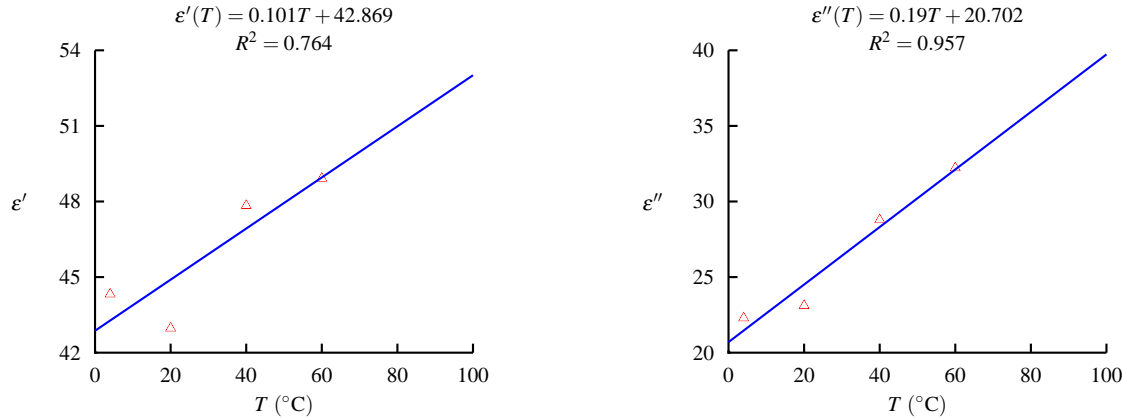


A.12 Cooked Ham

All values given here hold ONLY for $f = 2.45$ GHz, and assume 72% water content. Values for K hold for $0 \leq T \leq 60$. Values for c_0 and ρ are available only for $T = 20$. Cooked Ham will exhibit thermal runaway.

T (°C)	ϵ'	ϵ''	σ (S/m)	K (W/(m·°C))	c_0 (J/(kg·°C))	ρ (kg/m ³)
-20	6.944	1.857	0.253			
-10	10.000	4.286	0.584			
4	44.324	22.297	3.039	0.454		
20	42.973	23.108	3.150	0.454	2350	1070
40	47.838	28.784	3.923	0.454		
60	48.919	32.222	4.392	0.454		

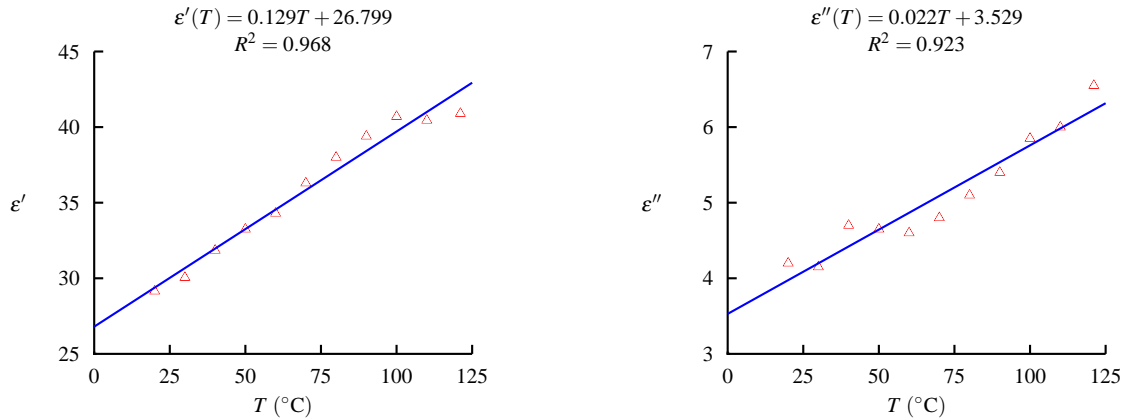
The linear fit described for ϵ' and ϵ'' uses only data for which $T \geq 0$ due to the large change in the behavior of these functions.



A.13 Cooked Macaroni Noodles

Values for K , c_0 , and ρ are not available for this material.

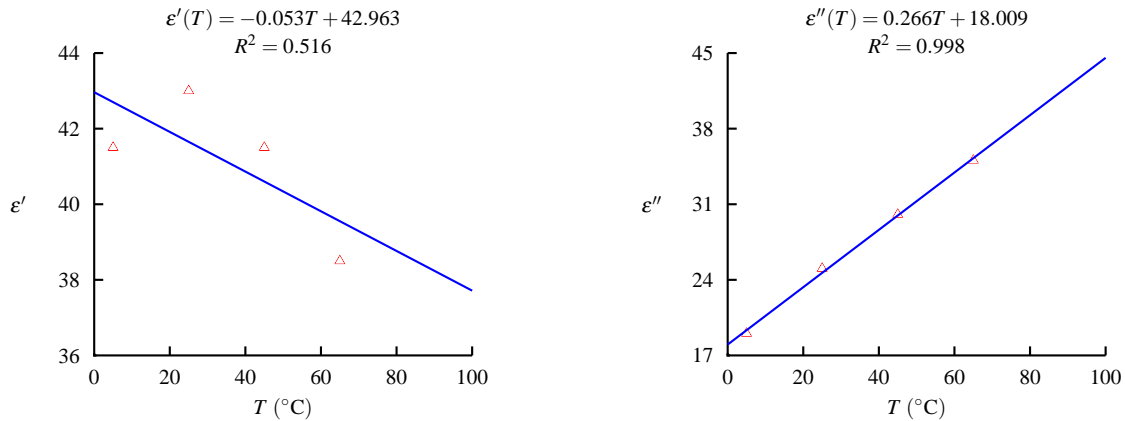
T (°C)	ϵ'	ϵ''	σ (S/m)	K (W/(m·°C))	c_0 (J/(kg·°C))	ρ (kg/m³)
20	29.15	4.20	0.214			
30	30.05	4.15	0.211			
40	31.85	4.70	0.239			
50	33.25	4.65	0.237			
60	34.30	4.60	0.234			
70	36.30	4.80	0.244			
80	38.00	5.10	0.260			
90	39.40	5.40	0.275			
100	40.70	5.85	0.298			
110	40.45	6.00	0.305			
121.1	40.90	6.55	0.333			



A.14 Cooked Turkey

Values for K , c_0 , and ρ are available only for $T = 25$.

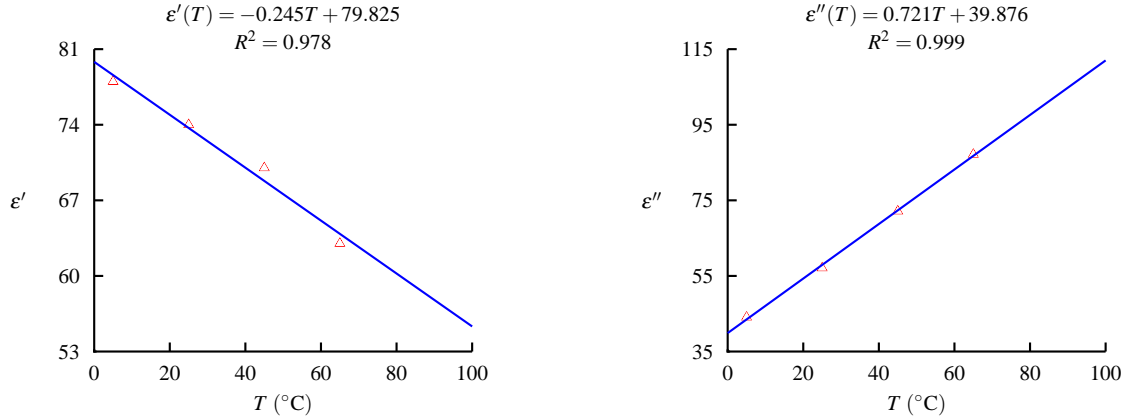
T (°C)	ϵ'	ϵ''	σ (S/m)	K (W/(m·°C))	c_0 (J/(kg·°C))	ρ (kg/m³)
5	41.5	19.036	0.969			
25	43.0	25.048	1.275	0.502	3310	1070
45	41.5	30.057	1.530			
65	38.5	35.067	1.785			



A.15 Cooked Turkey Juice

Values for K , c_0 , and ρ are not available for this material.

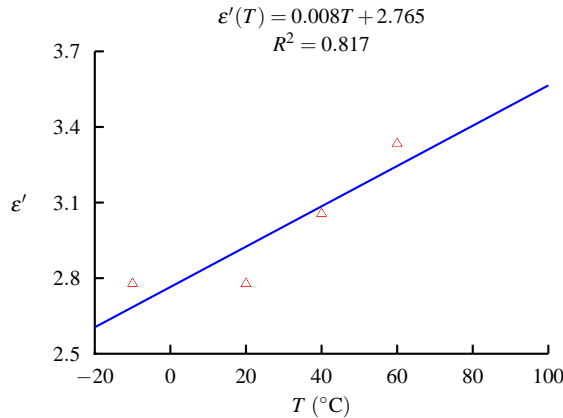
T (°C)	ϵ'	ϵ''	σ (S/m)	K (W/(m·°C))	c_0 (J/(kg·°C))	ρ (kg/m³)
5	78	44.084	2.244			
25	74	57.109	2.907			
45	70	72.138	3.672			
65	63	87.166	4.437			



A.16 Corn Oil

All data shown here holds ONLY for $f = 2.45$ GHz. Values for ϵ'' , σ , K , c_0 , and ρ are not available for this material.

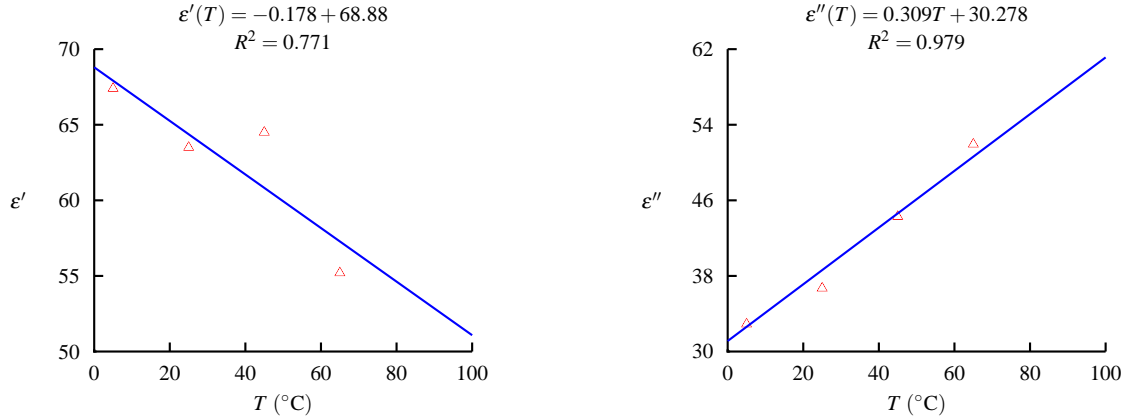
T (°C)	ϵ'	ϵ''	σ (S/m)	K (W/(m·°C))	c_0 (J/(kg·°C))	ρ (kg/m³)
-10	2.778					
20	2.778					
40	3.056					
60	3.333					



A.17 Cottage Cheese

Cottage cheese is assumed to be fat free. Values for K , c_0 and ρ are not available for this material.

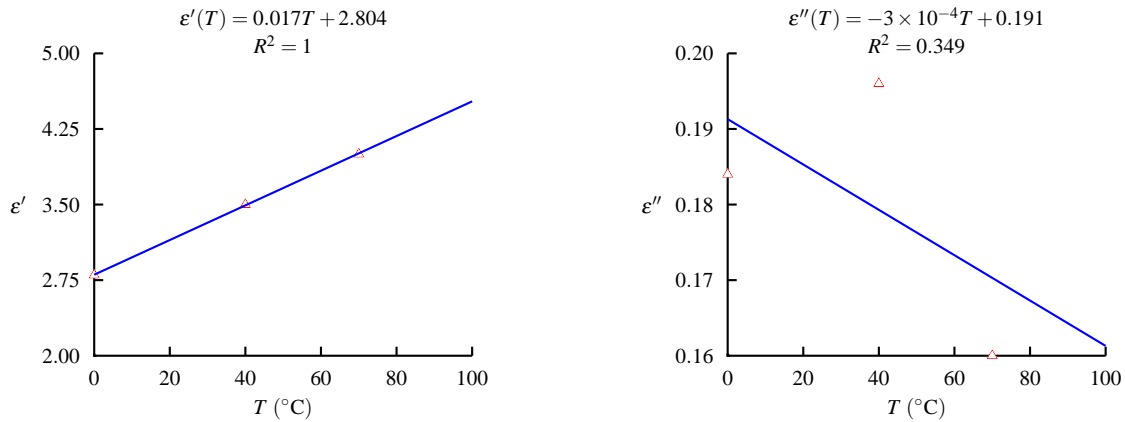
T ($^{\circ}\text{C}$)	ϵ'	ϵ''	σ (S/m)	K (W/(m \cdot $^{\circ}\text{C}$))	c_0 (J/(kg \cdot $^{\circ}\text{C}$))	ρ (kg/m 3)
5	67.4	32.9	1.675			
25	63.5	36.7	1.868			
45	64.5	43.5	2.214			
65	55.2	51.2	2.606			



A.18 Flour

All data given here holds ONLY for $f = 1$ GHz. These charts represent approximate behavior at $f = 915$ MHz. The flour is assumed to have a moisture content (MC) of 3.2%. Values for K , c_0 , and ρ are not available for this material.

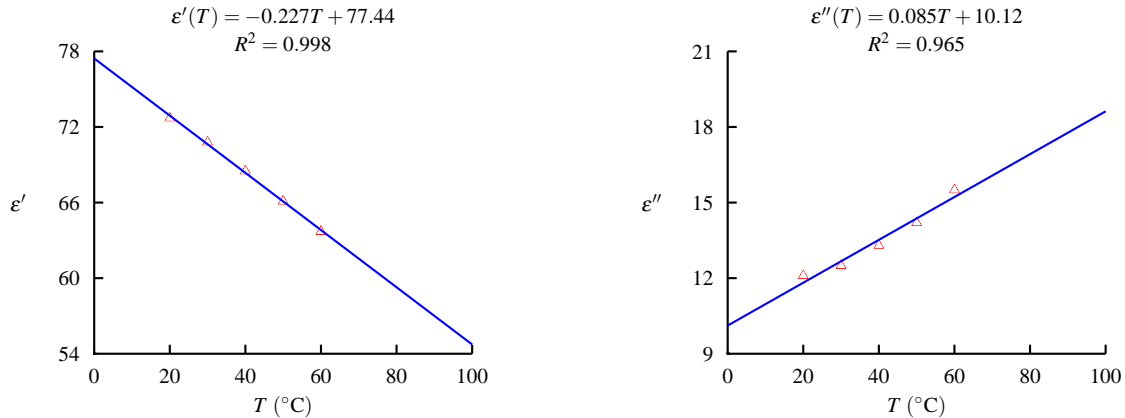
T ($^{\circ}\text{C}$)	ϵ'	ϵ''	σ (S/m)	K (W/(m \cdot $^{\circ}\text{C}$))	c_0 (J/(kg \cdot $^{\circ}\text{C}$))	ρ (kg/m 3)
0	2.8	0.184	0.010			
40	3.5	0.196	0.011			
70	4.0	0.160	0.009			



A.19 Grapefruit

Values for K , c_0 , and ρ are available only for $T = 20$.

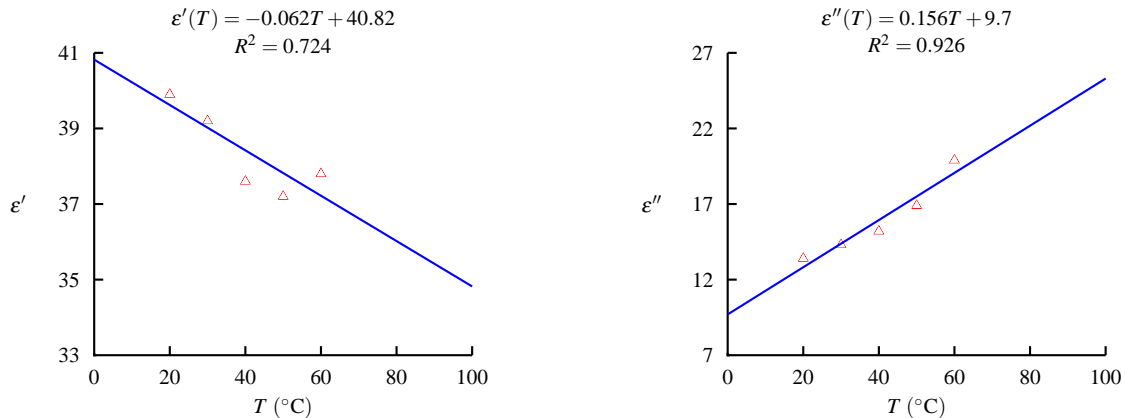
T (°C)	ϵ'	ϵ''	σ (S/m)	K (W/(m·°C))	c_0 (J/(kg·°C))	ρ (kg/m³)
20	72.7	12.1	0.616	0.549	3810	884
30	70.8	12.5	0.636			
40	68.5	13.3	0.677			
50	66.1	14.2	0.723			
60	63.7	15.5	0.789			



A.20 Indian-Meal Moth

Values for K , c_0 , and ρ are not available for this material.

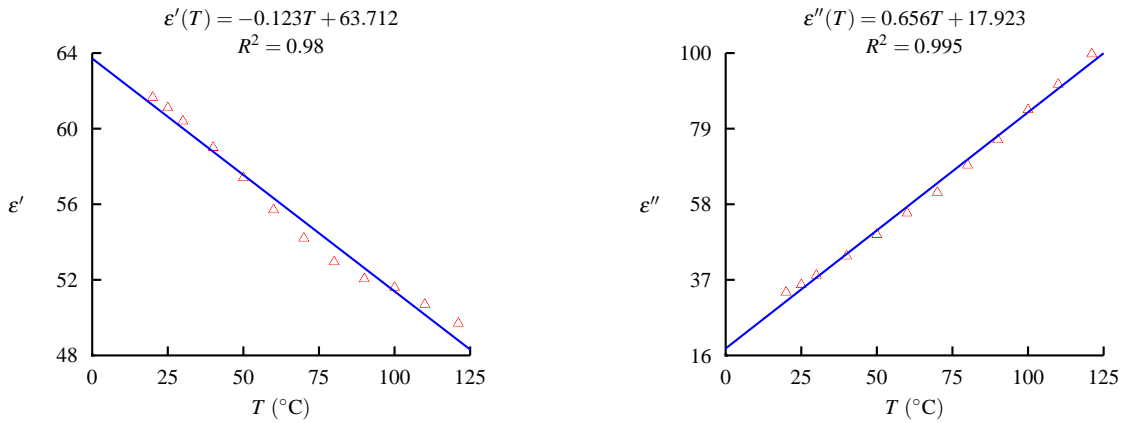
T (°C)	ϵ'	ϵ''	σ (S/m)	K (W/(m·°C))	c_0 (J/(kg·°C))	ρ (kg/m³)
20	39.9	13.4	0.682			
30	39.2	14.3	0.728			
40	37.6	15.2	0.774			
50	37.2	16.9	0.860			
60	37.8	19.9	1.013			



A.21 Liquid Whey Protein Mixture

Values for K , c_0 , and ρ are not available for this material.

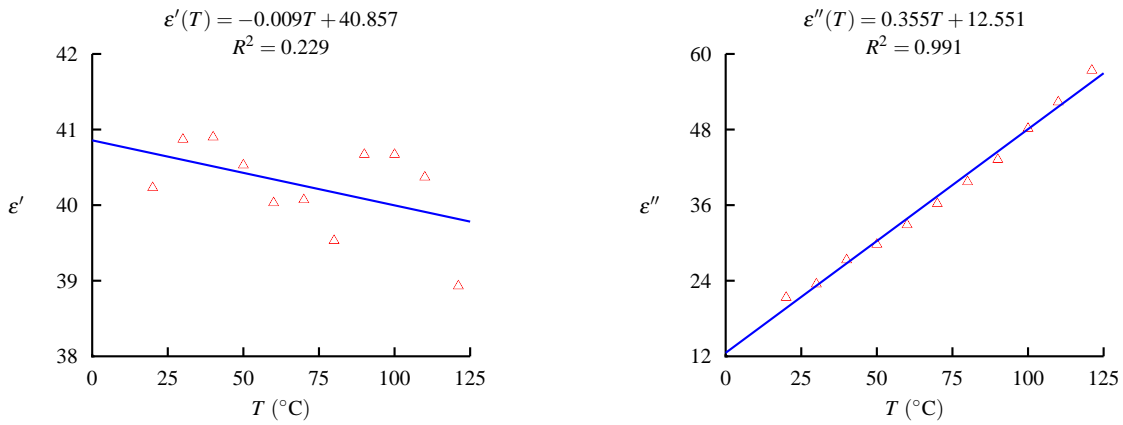
T (°C)	ϵ'	ϵ''	σ (S/m)	K (W/(m·°C))	c_0 (J/(kg·°C))	ρ (kg/m³)
20	61.65	33.55	1.708			
25	61.10	35.65	1.815			
30	60.40	38.25	1.947			
40	59.00	43.60	2.219			
50	57.40	49.55	2.522			
60	55.70	55.55	2.828			
70	54.20	61.30	3.120			
80	52.95	68.85	3.505			
90	52.05	75.90	3.864			
100	51.60	84.25	4.289			
110	50.70	91.30	4.647			
121.1	49.70	99.75	5.078			



A.22 Macaroni and Cheese

Values for K , c_0 , and ρ are not available for this material.

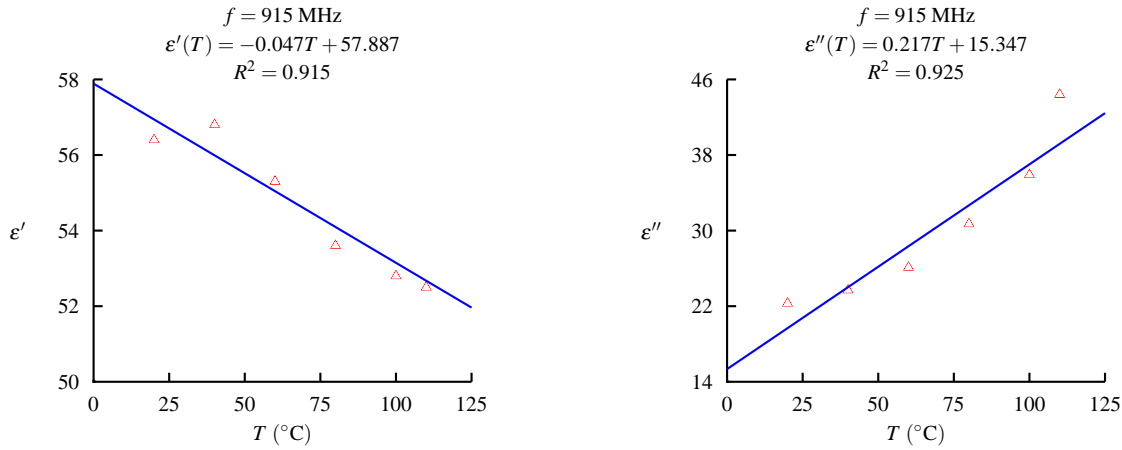
T (°C)	ϵ'	ϵ''	σ (S/m)	K (W/(m·°C))	c_0 (J/(kg·°C))	ρ (kg/m³)
20	40.23	21.33	1.086			
30	40.87	23.47	1.195			
40	40.90	27.30	1.390			
50	40.53	29.77	1.515			
60	40.03	32.87	1.673			
70	40.07	36.23	1.844			
80	39.53	39.70	2.021			
90	40.67	43.23	2.201			
100	40.67	48.17	2.452			
110	40.37	52.37	2.666			
121.1	38.93	57.40	2.922			



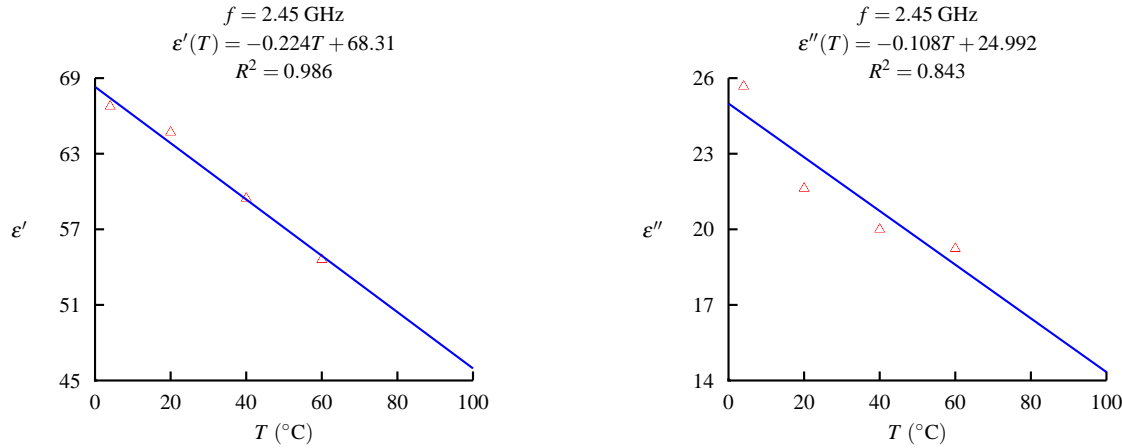
A.23 Mashed Potato

Material is assumed to have salt content of 0.8% and moisture content of 81.6%. Values for K , c_0 , and ρ are available only for $T = 20$ for both standard microwave oven frequencies.

$f = 915 \text{ MHz}$						
$T (\text{°C})$	ϵ'	ϵ''	$\sigma (\text{S/m})$	$K (\text{W}/(\text{m} \cdot \text{°C}))$	$c_0 (\text{J}/(\text{kg} \cdot \text{°C}))$	$\rho (\text{kg}/\text{m}^3)$
20	56.4	22.3	1.135	0.639	3640	1087
40	56.8	23.7	1.206			
60	55.3	26.1	1.329			
80	53.6	30.7	1.563			
100	52.8	35.9	1.827			
120	52.5	44.4	2.260			
$f = 2.45 \text{ GHz}$						
$T (\text{°C})$	ϵ'	ϵ''	$\sigma (\text{S/m})$	$K (\text{W}/(\text{m} \cdot \text{°C}))$	$c_0 (\text{J}/(\text{kg} \cdot \text{°C}))$	$\rho (\text{kg}/\text{m}^3)$
-20	5.000	0.714	0.097			
4	66.765	25.676	3.500			
20	64.706	21.622	2.947	0.639	3640	1087
40	59.459	20.000	2.726			
60	54.595	19.324	2.634			



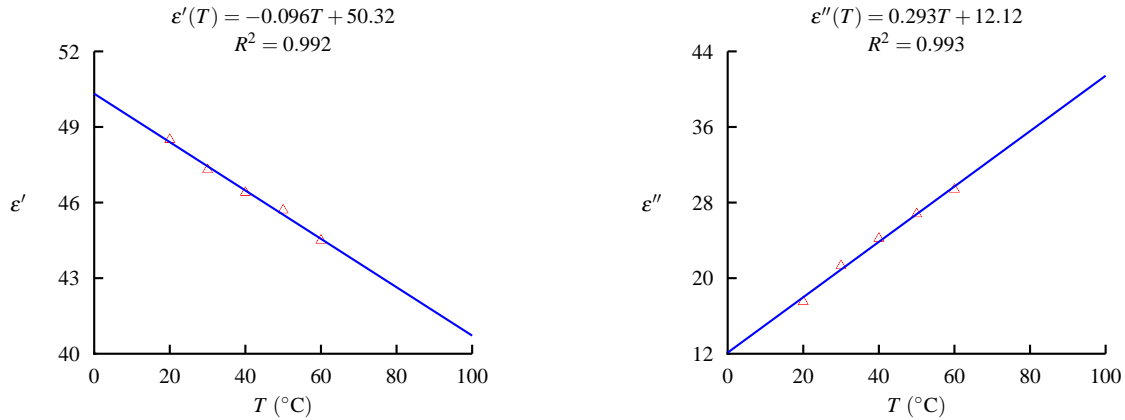
The linear fit described for ϵ' and ϵ'' for $f = 2.45 \text{ GHz}$ uses only data for which $T \geq 0$ due to the large change in the behavior of these functions.



A.24 Mexican Fruit Fly

Values for K , c_0 , and ρ are not available for this material.

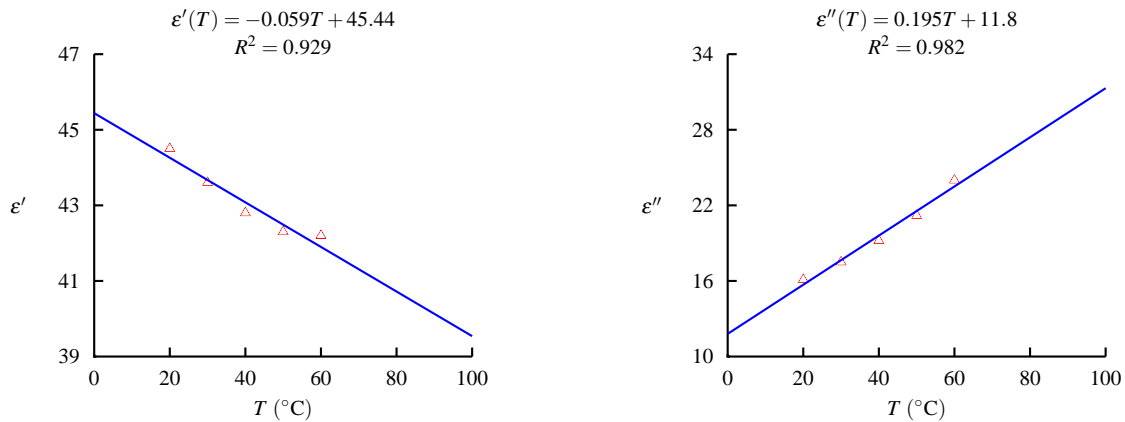
T (°C)	ϵ'	ϵ''	σ (S/m)	K (W/(m·°C))	c_0 (J/(kg·°C))	ρ (kg/m³)
20	48.5	17.5	0.891			
30	47.3	21.3	1.084			
40	46.4	24.2	1.232			
50	45.7	26.8	1.364			
60	44.5	29.4	1.497			



A.25 Naval Orange Worm

Values for K , c_0 , and ρ are not available for this material.

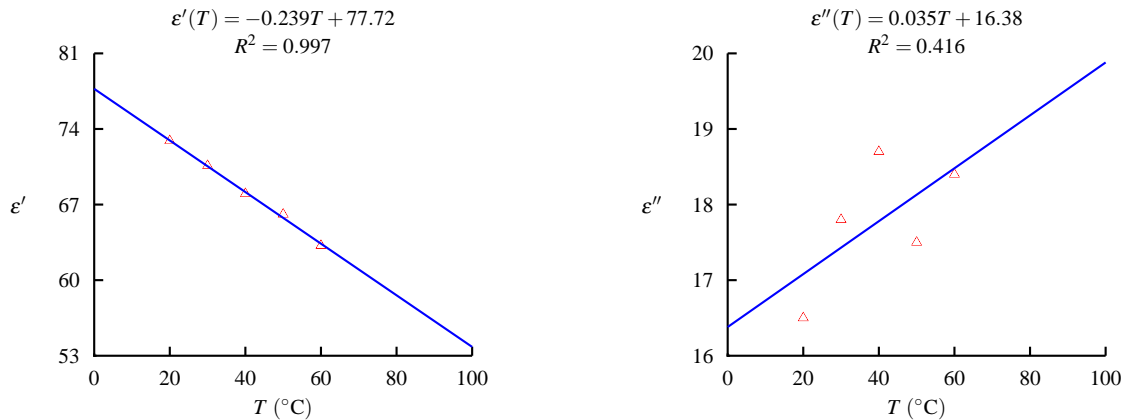
T (°C)	ϵ'	ϵ''	σ (S/m)	K (W/(m·°C))	c_0 (J/(kg·°C))	ρ (kg/m³)
20	44.5	16.1	0.820			
30	43.6	17.5	0.891			
40	42.8	19.2	0.977			
50	42.3	21.2	1.079			
60	42.2	24.0	1.222			



A.26 Orange

Values for K , c_0 , and ρ are available only for $T = 20$.

T (°C)	ϵ'	ϵ''	σ (S/m)	K (W/(m·°C))	c_0 (J/(kg·°C))	ρ (kg/m³)
20	72.9	16.5	0.840	0.58	3661	768
30	70.6	17.8	0.906			
40	68.0	18.7	0.952			
50	66.1	17.5	0.891			
60	63.2	18.4	0.937			



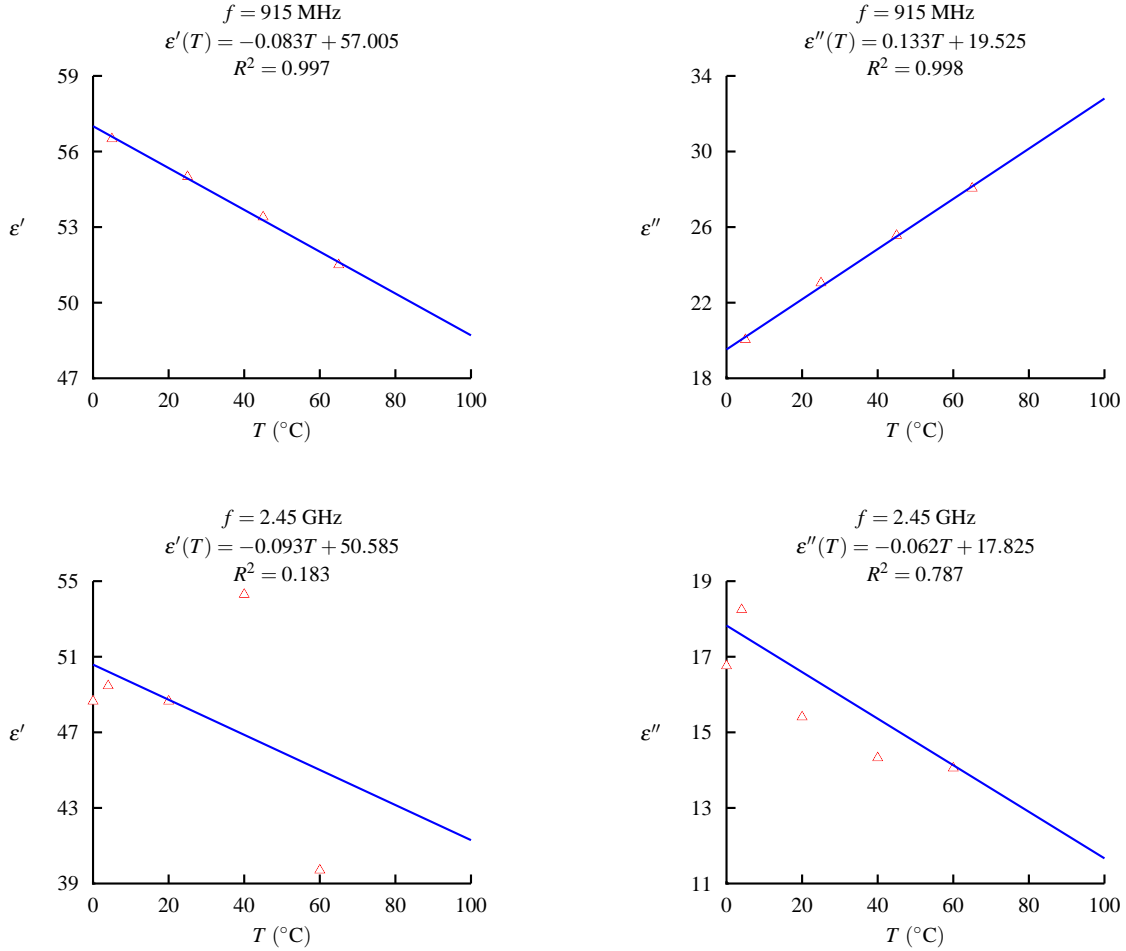
A.27 Raw Beef

All values given here assume 72% water content. All available data for both standard microwave oven frequencies is given below.

$f = 915 \text{ MHz}$						
T (°C)	ϵ'	ϵ''	σ (S/m)	K (W/(m·°C))	c_0 (J/(kg·°C))	ρ (kg/m³)
5	56.5	20.038	1.020		3431	
25	55.0	23.044	1.173	0.478	3431	
45	53.4	25.559	1.301		3431	
50				0.506	3431	
65	51.5	28.054	1.428		3431	
100				0.466	3431	
$f = 2.45 \text{ GHz}$						
T (°C)	ϵ'	ϵ''	σ (S/m)	K (W/(m·°C))	c_0 (J/(kg·°C))	ρ (kg/m³)
-20	4.177	0.571	0.078			
-10		1.429	0.195			
0	48.649	16.757	2.284		3431	
4	49.459	18.243	2.486		3431	
20	48.649	15.405 ¹	2.100		3431	
25				0.478	3431	
40	45.946	14.324	1.952		3431	
50				0.506	3431	
60	39.706	14.054	1.916		3431	
100				0.466	3431	

¹Two distinct values for ϵ'' were given for $T = 20$. A trend line also was given, which passed through the average of the two data points. The value of the trend line is given here.

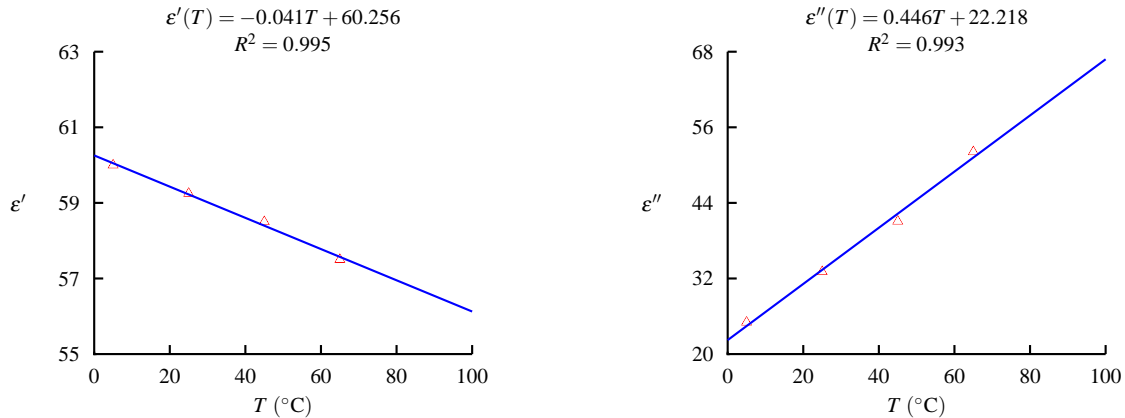
The linear fit described for ϵ' and ϵ'' for $f = 2.45$ GHz uses only data for which $T \geq 0$ due to the large change in the behavior of these functions.



A.28 Raw Turkey

Values for K , c_0 , and ρ are available only for $T = 25$.

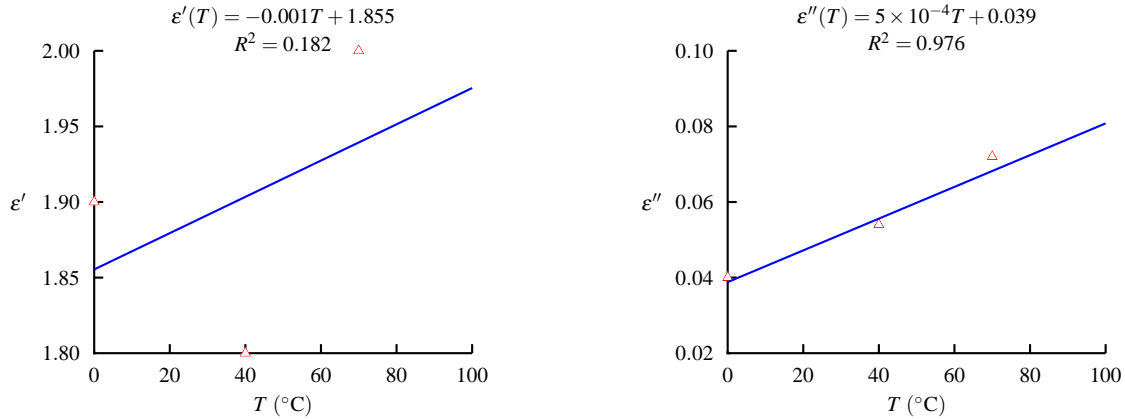
T ($^{\circ}\text{C}$)	ϵ'	ϵ''	σ (S/m)	K (W/(m \cdot $^{\circ}\text{C}$))	c_0 (J/(kg \cdot $^{\circ}\text{C}$))	ρ (kg/m 3)
5	60.00	25.048	1.275			
25	59.25	33.063	1.683	0.502	2810	1070
45	58.50	41.078	2.091			
65	57.50	52.099	2.652			



A.29 Skimmed Milk Powder

All data given here holds ONLY for $f = 1$ GHz, to be used only to approximate behavior at $f = 915$ MHz. Values for K , c_0 , and ρ are not available for this material.

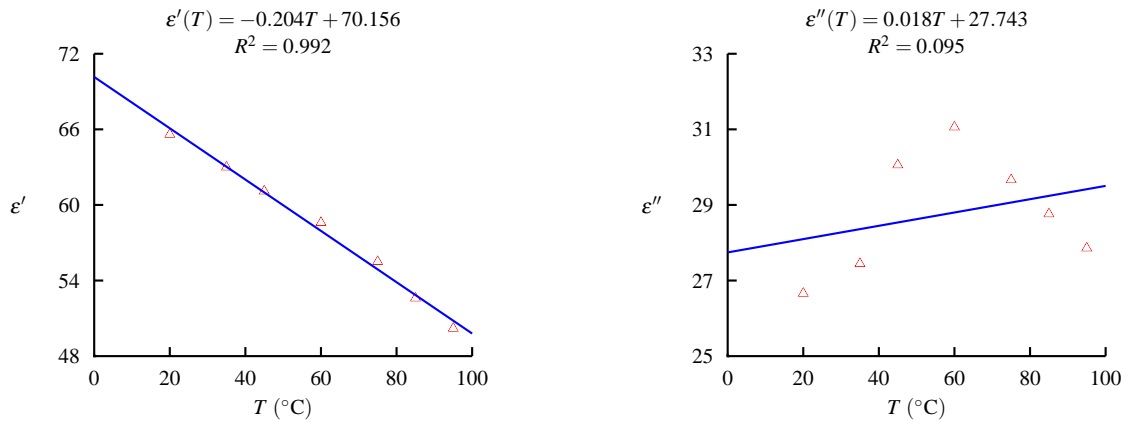
T (°C)	ϵ'	ϵ''	σ (S/m)	K (W/(m·°C))	c_0 (J/(kg·°C))	ρ (kg/m³)
0	1.9	0.040	0.002			
40	1.8	0.054	0.003			
70	2.0	0.072	0.004			



A.30 Solid Potato

Values for K , c_0 , and ρ are available only for $T = 20$.

T (°C)	ϵ'	ϵ''	σ (S/m)	K (W/(m·°C))	c_0 (J/(kg·°C))	ρ (kg/m³)
20	65.6	26.659	1.357	0.563	3515	1085
35	63.0	27.445	1.397			
45	61.1	30.057	1.530			
60	58.6	31.059	1.581			
75	55.5	29.664	1.510			
85	52.6	28.761	1.464			
95	50.2	27.857	1.418			



A.31 Tap Water

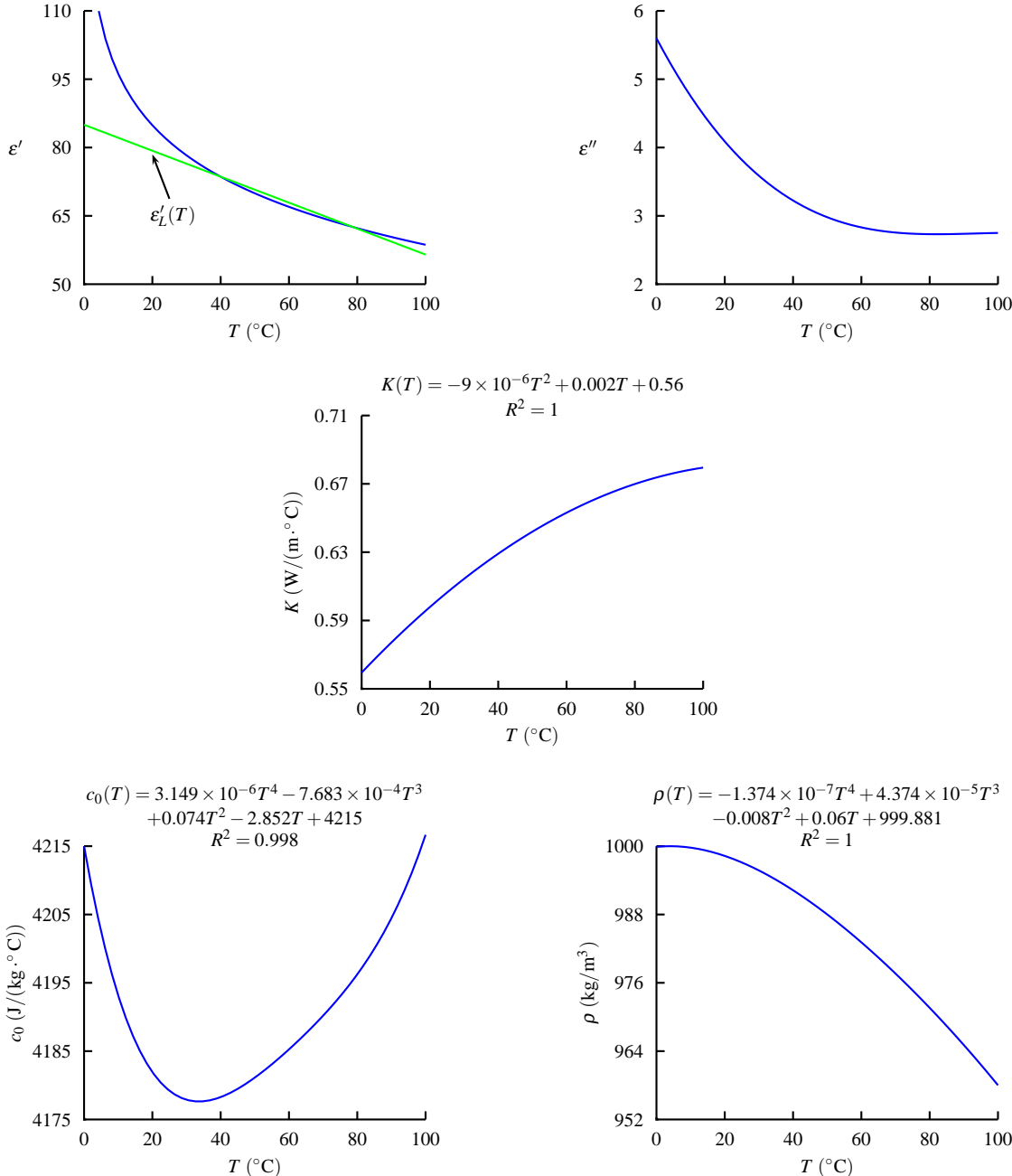
Using [6], we have the following *exact* equations that can be used to determine values for ϵ' and ϵ'' for tap water, assuming a pressure of 1 atm (normal atmospheric pressure at sea level at 0°C):

$$\begin{aligned}\epsilon'(T) &= -16.308 \ln T + 133.75 \\ \epsilon''(T) &= -3.68 \times 10^{-6} T^3 + 1.03 \times 10^{-3} T^2 - 0.095 T + 5.6.\end{aligned}$$

To avoid errors in FEMLAB when calculating values for ϵ' for $T < 0$, the following linearized approximation may be used:

$$\epsilon'_L(T) = -0.285T + 85.$$

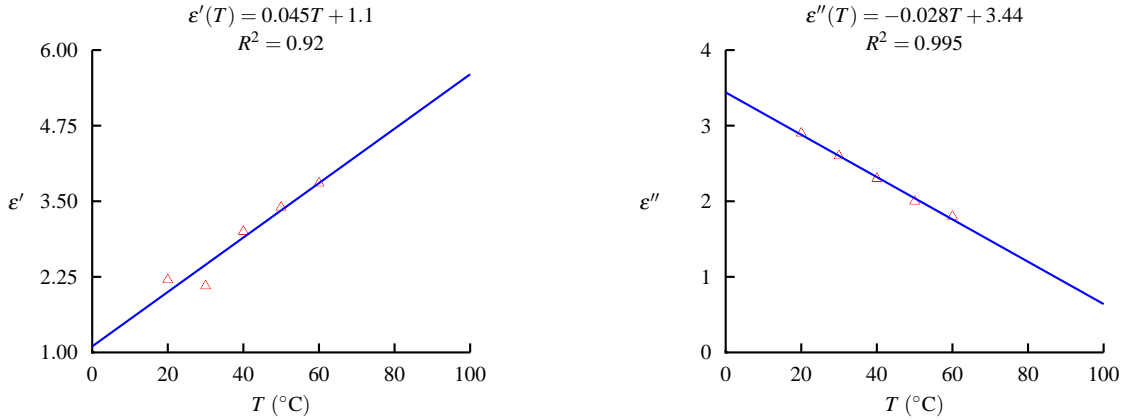
Values for K were available in 10°C increments, beginning with $T = 20$, plus $T = 25$. A nonlinear fit is used for this function. Values for c_0 and ρ were available in 1°C increments beginning with $T = 0$. As such, nonlinear fits are used for these functions as well, but a table of values is not provided here.



A.32 Walnut

Values for K , c_0 , and ρ are available only for $T = 20$.

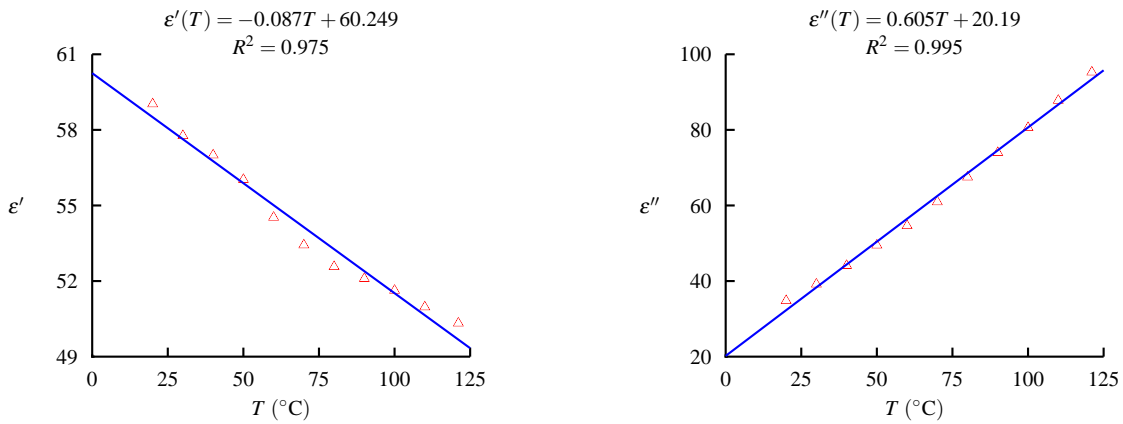
T (°C)	ϵ'	ϵ''	σ (S/m)	K (W/(m·°C))	c_0 (J/(kg·°C))	ρ (kg/m³)
20	2.2	2.9	0.148	0.127	1047	407
30	2.1	2.6	0.132			
40	3.0	2.3	0.117			
50	3.4	2.0	0.102			
60	3.8	1.8	0.092			



A.33 Whey Protein Gel

Values for K , c_0 , and ρ are not available for this material.

T (°C)	ϵ'	ϵ''	σ (S/m)	K (W/(m·°C))	c_0 (J/(kg·°C))	ρ (kg/m³)
20	59.03	34.80	1.771			
30	57.77	39.17	1.994			
40	57.00	44.10	2.245			
50	56.03	49.50	2.520			
60	54.53	54.63	2.781			
70	53.43	60.93	3.101			
80	52.57	67.50	3.436			
90	52.10	73.97	3.765			
100	51.63	80.57	4.101			
110	50.97	87.80	4.469			
121.1	50.33	95.27	4.849			



Appendix B

Notation Used

Throughout this report, we have attempted to use the standard notations, symbols, and units for all physical and mathematical quantities used in microwave power engineering, physics, and mathematics. However, to avoid confusion arising from possibly differing conventions among the disciplines, we have provided a listing of all symbols and notation used in this report, complete with the symbol, meaning, and units (if any).

Symbol	Meaning	Units
A	Wave amplitude constant. $A \in \mathbb{R}$ and $A \geq 0$. It is used in the explicit formulas for the \vec{E} - and \vec{H} -fields for TE and TM modes given in Chapter 2.	V/m
\mathbf{A}	The (unsymmetric) square system matrix used by FEMLAB in the direct and iterative solvers.	Arbitrary
\vec{A}	An arbitrary vector, used in the vector identity given in Chapter 2.	Arbitrary
\vec{B}	Magnetic flux intensity. $\vec{B} \in \mathbb{C}^3$ is a smooth 3D vector dependent on time: $\vec{B} = \vec{B}(t) = \langle B_x(t), B_y(t), B_z(t) \rangle$.	Wb/m ² = T
C	Specific heat capacity of a material. Used only in FEMLAB. See c_0 .	J/(kg · °C)
\vec{D}	Electric displacement, or electric flux density. Used in Maxwell's equations. $\vec{D} \in \mathbb{C}^3$ is a smooth 3D time-dependent vector: $\vec{D} = \vec{D}(t) = \langle D_x(t), D_y(t), D_z(t) \rangle$.	F · V/m ²
\vec{E}	Electric field intensity. $\vec{E} \in \mathbb{C}^3$ is a smooth 3D time-dependent vector: $\vec{E} = \vec{E}(t) = \langle E_x(t), E_y(t), E_z(t) \rangle$.	V/m
\vec{F}	An arbitrary Riemann-integrable vector function $\vec{F}(t) \in \mathbb{R}^3$. Used to illustrate the Divergence Theorem in Chapter 3.	Arbitrary
$H(t)$	Smoothed Heaviside step function. $H : \mathbb{R} \rightarrow \mathbb{R}$ and $H(t) = \begin{cases} 0 & t < -\varepsilon \\ p_7(t) & t < \varepsilon \\ 1 & t > \varepsilon \end{cases}$. Here, $\varepsilon > 0$ is a smoothing parameter and $p_7(t)$ is a 7 th -order polynomial such that $p_7(-\varepsilon) = 0$ and $p_7(\varepsilon) = 1$.	Dimensionless
\vec{H}	Magnetic field intensity. $\vec{H} \in \mathbb{C}^3$ is a smooth 3D vector dependent on time: $\vec{H} = \vec{H}(t) = \langle H_x(t), H_y(t), H_z(t) \rangle$.	A ² · Wb/(N · m ²)
\vec{J}	Electrical current. $\vec{J} \in \mathbb{C}^3$, and like \vec{E} , \vec{J} is a smooth 3D time-dependent vector function: $\vec{J} = \vec{J}(t) = \langle J_x(t), J_y(t), J_z(t) \rangle$	A
K	Thermal conductivity of a material. $K \in \mathbb{R}$ and $K \geq 0$. For some materials, it may be temperature-dependent; for others, constant. It is assumed to be isotropic.	W/(m · °C)
L_1, L_2	Length of the on and off cycles of a dynamically pulsed power function $P(t)$, respectively. $L_1 \in \mathbb{R}$, $L_2 \in \mathbb{R}$, $0 < L_1 \leq p$, and $0 < L_2 = p - L_1$.	s
P	Magnetron power output. This may be time-averaged or time-dependent. $P : \mathbb{R} \rightarrow \mathbb{R}$ and $P(t) \geq 0 \quad \forall t$.	W
P_v	Power absorbed by a load per unit volume. $P_v \in \mathbb{R}$ and $P_v \geq 0$.	W/m ³
Q_{av_weh}	Built-in time-averaged resistive heating term used in FEMLAB. See Q .	W/m ³

Q	Resistive heating. It is the heat source term used in the heat equation in Chapter 3. $Q \in \mathbb{R}$ and $Q \geq 0$.	W/m^3
S	An arbitrary 2D surface separating two dielectrics. Used in formulating the EM boundary conditions in Chapter 2.	m^2
\vec{S}	Poynting vector, giving the energy flux carried across a surface. $\vec{S} \in \mathbb{C}^3$ is a smooth 3D time-dependent vector function: $\vec{S} = \vec{S}(t) = \langle S_x(t), S_y(t), S_z(t) \rangle$.	W/m^2
T	Temperature of a material. T depends on location and time: $T : [0, a] \times [0, b] \times [0, \infty) \times [0, \infty] \rightarrow [-273.15, \infty)$.	$^\circ\text{C}$
\bar{T}	Average temperature of a material, independent of location but dependent on time: $\bar{T} = \bar{T}(t)$ and $\bar{T} : [0, \infty) \rightarrow (-273.15, \infty)$.	$^\circ\text{C}$
Z_{TE}	Electromagnetic wave impedance. This is the ratio of electric field strength to magnetic field strength.	Ω
a	Waveguide height, measured along the $+y$ -axis. $a \in \mathbb{R}$ and $a > 0$.	m
\hat{a}	A unit vector in an arbitrary direction. Used in formulating the exact solution to the vector wave equation in Chapter 2.	Dimensionless
$a_{i,j}$	Element located in the i^{th} row and j^{th} column of the system matrix \mathbf{A} .	Arbitrary
b	Waveguide width, measured along the $+x$ -axis. $b \in \mathbb{R}$ and $b > a > 0$.	m
c	Speed of light in free space. It is a constant, with standard value 2.998×10^8 .	m/s
c_0	Specific heat capacity of a material. It is the amount of energy needed to raise 1 unit of mass of a material by 1 unit of temperature. For some materials, it is temperature-dependent; for others, constant. $c_0 : [-273.15, \infty) \rightarrow (0, \infty)$.	$\text{J/(kg} \cdot {^\circ}\text{C)}$
d	Drop tolerance. Elements $a_{i,j}$ of the unsymmetric square system matrix \mathbf{A} with absolute value less than d will be converted to zero by FEMLAB.	Arbitrary
$d\ell$	Undirected infinitesimal line segment length, used in Chapter 2.	m
$d\vec{\ell}$	Directed infinitesimal line segment length, used in Chapter 2.	m
dm	Infinitesimal mass.	kg
dS	Undirected infinitesimal area of a surface S .	m^2
$d\vec{S}$	Directed infinitesimal area of a surface S , used in formulating the EM BCs in Chapter 2.	m^2
dV	Infinitesimal volume.	m^3
e	Napierian logarithm base. It is a constant, with approximate value 2.718285.	Dimensionless
f	Applied wave frequency. $f \in \mathbb{R}$ and $f \geq 0$. Unless specified to be arbitrary, we use a value of 9.15×10^8 .	Hz
i	Imaginary unit, equal to $\sqrt{-1}$.	Dimensionless
j	Imaginary unit used in FEMLAB. $j = i$.	Dimensionless
\hat{k}	Standard unit vector in the $+z$ -direction.	Dimensionless
l	Number of half waves in the $+x$ -direction contained in a waveguide of width b for a TE, TM, or TEM wave. $l \in \mathbb{N} \cup \{0\}$.	Dimensionless
m	Number of half waves in the $+y$ -direction contained in a waveguide of height a for a TE, TM, or TEM wave. $m \in \mathbb{N} \cup \{0\}$. In this context, l and m cannot both be zero.	Dimensionless
m	Mass of a material. Used only in formulating the heat equation in Chapter 3. $m \in \mathbb{R}$ and $m > 0$.	kg
\hat{n}	An outward unit normal vector, used in formulating both the EM and heat BCs in Chapters 2 and 3.	Dimensionless
p	Period of a pulse. Used in describing pulsing functions for $P(t)$ in Chapter 5. $p \in \mathbb{R}$ and $p > 0$.	s
\vec{q}	Fourier heat flux vector, appearing in Fourier's Law of Conduction. $\vec{q} \in \mathbb{R}^3$ is a smooth 3D time-dependent vector function: $\vec{q} = \vec{q}(t) = \langle q_x(t), q_y(t), q_z(t) \rangle$.	W/m^2
\vec{r}	Position vector. $\vec{r} \in \mathbb{R}^3$ and $\vec{r} = \langle x, y, z \rangle$.	m
s_{\max}	Nyquist maximum element size of a material. $s_{\max} \in \mathbb{R}$ and $s_{\max} > 0$.	m
t	Elapsed time. $t \in \mathbb{R}$ and $t \geq 0$.	s
x	Position from the origin along the waveguide width. Here, $x \in \mathbb{R}$ and $0 \leq x \leq b$.	m

y	Position from the origin along the waveguide height. Here, $y \in \mathbb{R}$ and $0 \leq y \leq a$.	m
z	Position from the origin along the waveguide length. Here, $z \in [0, \infty)$.	m
Ω	An arbitrary 3D volumetric domain. $\Omega \subset \mathbb{R}^3$	m^3
$\partial\Omega$	An arbitrary 2D surface domain which bounds the volumetric domain Ω . $\partial\Omega \subset \mathbb{R}^2$.	m^2
α^2	Thermal diffusivity of a material, appearing in the 3D heat equation. It is assumed to be constant for all materials except for tap water, in which it is temperature-dependent: $\alpha^2 : (-273.15, \infty) \rightarrow [0, \infty)$.	m^2/s
β	Electromagnetic wave propagation constant used in FEMLAB. $\beta \in \mathbb{R}$ and $\beta = \kappa_n$	$1/\text{m}$
δ	Dielectric loss tangent angle, measured in radians. $\delta \in [0, \pi/2)$.	Dimensionless
δ_{ts}	Time-scaling coefficient. Used in FEMLAB's heat equation. $\delta_{ts} = 1$ for every numerical experiment conducted by us.	Dimensionless
ϵ	Complex permittivity of a material. $\epsilon \in \mathbb{C}$ and $\epsilon = \epsilon' - i\epsilon''$.	Dimensionless
ϵ'	Relative permittivity or dielectric constant of a material. $\epsilon' = \text{Re}(\epsilon)$ and $\epsilon' \geq 0$.	Dimensionless
ϵ''	Dielectric loss factor of a material. $\epsilon'' = \text{Im}(\epsilon)$ and $\epsilon'' \geq 0$.	Dimensionless
ϵ_r	Relative permittivity used in FEMLAB. $\epsilon_r = \epsilon'$.	Dimensionless
ϵ_0	Electrical permittivity of free space. It is a constant, valued at 8.854×10^{-12} .	F/m
κ_c	Cutoff wavenumber, below which no EM wave will propagate without attenuation. It is dependent on the cutoff frequency and mode.	$1/\text{m}$
κ_n	Propagation constant, or wavenumber in the direction of \hat{n} , equal to $2\pi/\lambda_n$.	$1/\text{m}$
κ_x	Wavenumber in the $+x$ -direction, equal to $2\pi/\lambda_x$.	$1/\text{m}$
κ_y	Wavenumber in the $+y$ -direction, equal to $2\pi/\lambda_x$.	$1/\text{m}$
κ_z	Wavenumber in the $+z$ -direction. $\kappa_z \in \mathbb{R}$.	$1/\text{m}$
κ_0	Wavenumber used in FEMLAB's EM wave equation in place of ω/c . $\kappa_0 \in \mathbb{R}$ and $\kappa_0 > 0$.	$1/\text{m}$
λ	Wavelength of an EM wave. $\lambda \in \mathbb{R}$ and $\lambda > 0$.	m
μ'	Relative permeability of a material. $\mu' \in \mathbb{R}$ and $\mu' \geq 0$. $\mu' = 1$ for every numerical experiment we conduct. It is assumed to be isotropic.	Dimensionless
μ_r	Relative permeability used in FEMLAB. $\mu_r = \mu'$.	Dimensionless
μ_0	Magnetic permeability of a material. It is a constant, defined <i>exactly</i> as $4\pi \times 10^{-7}$.	N/A^2
v	Speed of light in a medium. $v \neq c$ if light is not traveling in free space. $v \in \mathbb{R}$ and $v > 0$.	m/s
π	Archimedes' constant, with approximate value 3.141592654.	Dimensionless
ρ	Electrical charge density, appearing in Maxwell's equations in Chapter 2. It is assumed to be isotropic.	C/m^3
ρ	Mass density of a material, used in Chapters 3 through 5 as well as in Appendix A. For some materials, it is constant; for others, temperature-dependent: $\rho : (-273.15, \infty) \rightarrow (0, \infty)$. It is assumed to be isotropic.	kg/m^3
σ	Electrical conductivity of a material. It is temperature-dependent: $\sigma : (-273.15, \infty) \rightarrow [0, \infty)$.	S/m
ϕ	Plane wave amplitude, used in solving the Helmholtz equation. $\phi : [0, b] \times [0, a] \rightarrow \mathbb{R}$	V
χ	Wave phase constant, appearing in the general solution to the Helmholtz equation. It determines phase-shifting of the wave. $\chi \in \mathbb{R}$.	Dimensionless
ψ	Time-harmonic solution to the scalar wave equation. It has spatial and temporal dependencies: $\psi : [0, b] \times [0, a] \times [0, \infty) \times [0, \infty) \rightarrow \mathbb{C}$	V
ω	Angular wave frequency. $\omega \in \mathbb{R}$ and $\omega > 0$.	Hz

Bibliography

- [1] R. V. Churchill and J. W. Brown. *Fourier Series and Boundary Value Problems*. McGraw-Hill, New York, third edition, 1978.
- [2] W. C. Elmore and M. A. Heald. *Physics of Waves*. Dover, New York, 1985.
- [3] D. Guan, M. Cheng, Y. Want, and J. Tang. Dielectric Properties of Mashed Potatoes Relevant to Microwave and RF Pasteurization and Sterilization Processes. *Journal of Food Science*, 69(1):E30–E38, January/February 2004.
- [4] A.-G. Herve, J. Tang, L. Luedcke, and H. Feng. Dielectric Properties of Cottage Cheese and Surface Treatment using Microwaves. *Journal of Food Engineering*, 37(4):389–410, September 1998.
- [5] J. Jin. *The Finite Element Method in Electromagnetics*. Wiley–IEEE, second edition, 2002.
- [6] V. V. Komarov and J. Tang. Dielectric Permittivity and Loss Factor of Tap Water at 915 MHz. *Microwave and Optical Technology Letters*, 42(5):419–420, September 2004.
- [7] V. V. Komarov, S. Wang, and J. Tang. Permittivity and Measurement. In K. Chang, editor, *The Wiley Encyclopedia of RF and Microwave Engineering*. Wiley, New York, 2005.
- [8] S. Nekrutman and I. Rogov. *Microwave Heating of Food Product*. Agropromizdat, Moscow, second edition, 1986.
- [9] J. M. Osepchuk. A History of Microwave Heating Applications. *IEEE Transactions on Microwave Theory and Techniques*, 32(9):1200–1224, September 1984.
- [10] J. Thuéry. *Microwaves: Industrial, Scientific, and Medical Applications*. Artech House, Boston, 1992.
- [11] E. To, R. Mudgett, D. Wang, S. Goldblith, and R. Decareau. Dielectric Properties of Food Materials. *Journal of Microwave Power*, 9(4):303–316, 1974.
- [12] Y. Wang, T. D. Wig, J. Tang, and L. M. Hallberg. Dielectric Properties of Foods Relevant to RF and Microwave Pasteurization and Sterilization. *Journal of Food Engineering*, 57(3):257–268, May 2003.